PCCP

Accepted Manuscript

This article can be cited before page numbers have been issued, to do this please use: M. L. Gill, A. Byrd and A. G. Palmer, III, *Phys. Chem. Chem. Phys.*, 2015, DOI: 10.1039/C5CP06197K.

ROYAL SOCIETY OF CHEMISTRY

www.rsc.org/pccp

View Article Online
DOI: 10.1039/C5CP06197K

Dynamics of GCN4 Facilitate DNA Interaction: A Model-Free Analysis of an Intrinsically Disordered Region

Michelle L. Gill,[1,2] R. Andrew Byrd,[2] and Arthur G. Palmer, III[1*]

[1]Department of Biochemistry and Molecular Biophysics

Columbia University

New York, NY 10032

[2]Structural Biophysics Laboratory

National Cancer Institute

National Institutes of Health

Frederick, MD 21702

[*]Address correspondence to:

Arthur G. Palmer, III

Tel: (212) 305-8675

Fax: (212) 305-7932

Email: agp6@columbia.edu

View Article Online
DOI: 10.1039/C5CP06197K

Abstract

Intrinsically disordered proteins (IDPs) and proteins with intrinsically disordered regions (IDRs) are known to play important roles in regulatory and signaling pathways. A critical aspect of these functions is the ability of IDP/IDRs to form highly specific complexes with target molecules. However, elucidation of the contributions of conformational dynamics to function has been limited by challenges associated with structural heterogeneity of IDP/IDRs. Using NMR spin relaxation parameters (^{15}N R_1, ^{15}N R_2, and $\{^1H\}$-^{15}N heteronuclear NOE) collected at four static magnetic fields ranging from 14.1 to 21.1 T, we have analyzed the backbone dynamics of the basic leucine-zipper (bZip) domain of the *Saccharomyces cerevisiae* transcription factor GCN4, whose DNA binding domain is intrinsically disordered in the absence of DNA substrate. We demonstrate that the extended Model-free analysis can be applied to proteins with IDRs such as *apo* GCN4 and that these results significantly extend previous NMR studies of GCN4 dynamics performed using a single static magnetic field of 11.74 T [Bracken, *et al*. (1999) *J. Mol. Biol*., 285, 2133–2146] and correlate well with molecular dynamics simulations [Robustelli, *et al.* (2013) *J. Chem. Theory Comput.*, 9, 5190–5200]. In contrast to the earlier work, data at multiple static fields allows the time scales of internal dynamics of GCN4 to be reliably quantified. Large amplitude dynamic fluctuations in the DNA-binding region have correlation times ($\tau_s \approx$ 1.4–2.5 ns) consistent with a two-step mechanism in which partially ordered bZip conformations of GCN4 form initial encounter complexes with DNA and then rapidly rearrange to the high affinity state with fully formed basic region recognition helices.

View Article Online
DOI: 10.1039/C5CP06197K

Introduction

The discovery of intrinsically disordered proteins (IDPs) and proteins with extensive intrinsically disordered regions (IDRs), collectively referred to as IDPs herein, challenged the structure-function paradigm by demonstrating that biological activity is possible in the absence of well-defined tertiary structure [1,2]. In the time since this discovery, sequence analyses have led to the realization that IDPs are widely distributed: recent estimates suggest that over 100,000 disordered regions are located throughout ~40% of the mammalian proteome [1,3,4]. Moreover, IDPs are associated with crucial but diverse roles in cellular function, including signaling pathways [5,6], cell cycle regulation [5,7], and control of both transcription and translation [2,8,9].

The mechanisms by which IDPs recognize and bind to their substrates or interaction partners are central to their biochemical properties. Two limiting paradigms have been proposed. The first, conformational selection, posits that more-ordered, binding-competent structures exist among an ensemble of conformations and that these conformers are selected during the binding process [10,11]. The second, induced fit, posits that binding-competent structures are induced by interactions with the target [2,12]. Biochemical, theoretical, and computational evidence suggests these two alternatives are the extremes of a spectrum of behavior, rather than independent dichotomies [13-15].

Structural variability and dynamic substrate interaction mechanisms make IDPs well-suited to rapid control of cellular processes. For example, the extremely fast (often diffusion-limited) association rates for transcription factors enables fast activation of the signaling response [6,16]. Likewise, the tendency of IDPs to bind partners or ligands with high specificity but modest affinity leads to rapid dissociation, and thus signal termination [17,18].

View Article Online
DOI: 10.1039/C5CP06197K

The transient and flexible (structurally heterogeneous) nature of IDPs creates challenges for their study by techniques of structural biology. Crystallization of IDPs, particularly in their unbound (disordered) states, often is not possible. Considerable success has been reported using NMR methods to study IDPs [19,20], but the absence of a single, global correlation time hinders application of approaches such as the Model-free formalism [21,22] as a method for analyzing otherwise powerful NMR spin relaxation measurements. We demonstrate herein that an extended protocol and analysis can overcome these limitations and provide a general approach for the detailed examination of internal dynamics in IDPs.

The *Saccharomyces cerevisiae* protein GCN4, which has homologs in mammals [23], is a prototypical example of a transcription factor that binds DNA target sequences using IDRs. The DNA-binding domain of GCN4, termed the bZip domain, contains an N-terminal highly basic helical region that inserts into the DNA major groove and a C-terminal region that dimerizes to form a leucine zipper (Figure 1A) [24,25]. In the absence of DNA substrate, the N-terminal region consists of a (partially) disordered ensemble (Figure1B) that contains significant residual helicity [26-29], while the C-terminal leucine zipper remains ordered and dimeric under the solution conditions used in the present work. The presence of both a flexible and an ordered region makes GCN4 an ideal model for demonstration of the proposed formalism.

Using NMR spin relaxation measurements (^{15}N R_1, ^{15}N R_2, and $\{^1H\}$-^{15}N heteronuclear NOE) for backbone amide moieties, collected at four static magnetic fields, we have performed spectral density mapping and Model-free analysis on the *apo* (substrate-free) form of the GCN4 bZip domain. The order parameters (S^2) are consistent with previous studies, including an analysis of ^{15}N spin relaxation data from a single static field [26] and recent molecular dynamics simulations [30]. Significantly, the use of multiple static fields allowed internal motions to be

View Article Online
DOI: 10.1039/C5CP06197K

resolved on ps and ns timescales, which was not possible previously. The disordered basic domain contains regions with motions whose correlation times are consistent with structural pre-organization in advance of DNA substrate binding followed by rapid stabilization within the DNA encounter complex. Thus, the GCN4 bZip domain utilizes aspects of both selected- and induced-fit binding mechanisms. This may be a common paradigm for IDPs, which can now be investigated in detail using the strategy described herein.

Methods

Sample preparation

The DNA binding domain of *Saccharomyces cerevisiae* GCN4 was expressed and purified as described previously [26]. Briefly, BL21(DE3)-pLysS cells were transformed and grown in 1–2 L of M9 minimal media with 1 g/L $^{15}NH_4Cl$ and either 4 g/L of unlabeled glucose in 98% $^{2}H_2O$ or 4 g/L $^{13}C_6$-glucose in H_2O at 37 °C to an optical density (OD_{600}) of 0.7. Protein expression was induced with 1 mM IPTG and allowed to proceed for approximately 2 hrs. The protein was purified on an SP sepharose column with 25 mM HEPES, pH 7.5, and 1 mM EDTA with a gradient of 0.2–1 M NaCl followed by HPLC purification using a C18 reverse phase column with starting buffer of 10% acetonitrile/0.1% trifluroacetic acid (TFA) and final buffer of 90% acetonitrile/0.1 % TFA. Eluted fractions were lyophilized and then reconstituted into a pH 4.5 buffer that contained 50 mM sodium acetate-d_6, and 75 mM KCl in 90%H_2O/10% $^{2}H_2O$ [26]. Final GCN4 sample concentrations were 1 mM U-[^{15}N, ^{13}C] and 800 μM U-[^{15}N, ^{2}H], respectively. Protein concentrations are defined with respect to a single monomer.

View Article Online
DOI: 10.1039/C5CP06197K

NMR spectroscopy

NMR experiments were conducted on Bruker Avance spectrometers operating at 14.1, 16.45, 18.8, and 21.1 T. The spectrometer operating at 16.45 T was equipped with a triple resonance, triple-axis gradient room temperature probe. All other spectrometers were equipped with triple resonance *z*-axis gradient TCI cryoprobes. Sample temperature was calibrated at 300 K with 98% $^{2}H_4$-methanol as described previously [31].

Resonance assignments [26] were confirmed using HNCA [32-34] and HN(CO)CA spectra [32,34] with 12.6 × 2.9 × 7.3 kHz spectral widths and 1024 × 30 × 64 complex points ($t_3 \times t_2 \times t_1$), and a 3D ($^{1}H$, ^{15}N, ^{15}N) HSQC-NOESY-HSQC [35,36] with 10.8 × 2.1 × 2.4 kHz spectral widths, 1024 × 64 × 64 complex points, and 600 ms mixing time. All assignment experiments were collected with 16 scans at 21.1 T.

R_1, R_2, and $\{^{1}H\}$-^{15}N heteronuclear NOE experiments [37,38] were recorded with spectral widths of 7.2 × 1.6, 8.4 × 1.8, 9.6 × 2.1, and 10.8 × 2.4 kHz for 14.1, 16.45, 18.8 and 21.1 T, respectively, and contained 1024 × 300 complex points. Relaxation delays for the R_1 and R_2 experiments ranged from 0.02–1.75 and 0.004–0.208 s, respectively, and are listed for each static magnetic field in Table S1. For the R_2 experiment, the phase cycle of Yip and Zuiderweg [39] was incorporated in the CPMG train for improved off-resonance compensation and the spacing between 180° pulses was 500 μs. The R_1 and R_2 experiments were collected with 8 scans per FID. The heteronuclear NOE experiment was collected with 32 scans, and the t_1 points of the Boltzmann and saturation experiments were interleaved during acquisition. The R_1 and R_2 experiments used the Rance-Kay protocol and the NOE experiments used the States-TPPI protocol for quadrature detection [40-43].

View Article Online
DOI: 10.1039/C5CP06197K

Data processing and analysis

All data were processed in NMRPipe [44]. The two indirect dimensions of the HNCA, HN(CO)CA, and HSQC-NOESY-HSQC experiments were processed with linear prediction and a Kaiser window ($\theta = \pi$) in the two indirect dimensions. The relaxation data were processed using a Kaiser window ($\theta = \pi$) for t_1 and linear prediction with 3 Hz exponential line broadening for t_2. Resonance assignments and quantitation of peak intensities were performed in Sparky [45]. Additional data processing and visualization was performed using the Python scientific libraries [46-52].

Determination of relaxation parameters

The program *relax* [53,54], version 3.2.3, was used for determination of relaxation parameters. Errors in R_1 and R_2 rate constants were determined from 500 Monte Carlo simulations, while those for the heteronuclear NOE were calculated from the noise floor. Due to large variations in peak intensities between disordered and coiled-coil regions, relaxation parameters were analyzed in two separate groups (residues 1–12 and 56–58 for disordered residues and 13–55 for ordered residues), as determined by k-means clustering of initial R_1 and R_2 peak intensities. Five residues were omitted from analysis due to spectral overlap (31, 33, 34, 36, 40, and 47), residue 2 was not quantified because its extremely narrow resonance lineshape was not well-digitized, and residue 4 is a proline. The resulting R_2 rates were corrected for R_1 contribution as described by Yip and Zuiderweg [39].

The 10% trimmed mean correlation time (τ_M) and diffusion tensor anisotropy for the coiled-coil region were calculated at each static field from the ratio R_2/R_1 and Model-free local correlation times (τ_M), respectively, using the program quadric [55,56]. The mean correlation time

View Article Online
DOI: 10.1039/C5CP06197K

for data recorded at 16.45 T was 15.6 ns, lower than the mean value of 16.9 ns for the other fields (14.1, 18.8, and 21.1 T). This difference likely reflects a slightly elevated sample temperature for the 16.45 T (700 MHz) NMR spectrometer, as it was the only instrument with a room-temperature probe. To account for this difference, R_1 and R_2 relaxation rates recorded at 16.45 T were adjusted for the difference in τ_M according to the following equations:

$$R_1 = R_{10}(\tau_M / \tau_{M0})(1+\omega_N^2\tau_{M0}^2)/(1+\omega_N^2\tau_M^2)$$
$$R_2 = (R_{20} - 0.5R_{10})(\tau_M / \tau_{M0}) + 0.5R_1 \qquad 1$$

where ω_N is the ^{15}N frequency at 16.45 T. R_{10}, R_{20}, and τ_{M0} are the respective original R_1 and R_2 relaxation rates and correlation time, and R_1, R_2, and τ_M are the adjusted versions. In addition, the uncertainties in R_1, R_2, and heteronuclear NOE data were rescaled by an empirical factor of 1.38 so the median χ^2 of the combined linear regressions of Γ_{auto} vs $(3d^2 + 4c^2)/6$, $J(\omega_N)$ vs ω_N^{-2}, and $J(0.870\omega_H)$ vs $(0.870\omega_H)^{-2}$ was equal to 1.0 (*vide infra*). These two adjustments reduced the χ^2 values in subsequent Model-free analyses of the relaxation data but did not significantly change the fitted parameter values or selected models.

Spectral density mapping

The ^{15}N relaxation rate constants are given by:

$$R_1 = (d^2/4)\{J(\omega_H - \omega_N) + 3J(\omega_N) + 6J(\omega_H + \omega_N)\} + c^2 J(\omega_N)$$
$$R_2 = (d^2/8)\{4J(0) + J(\omega_H - \omega_N) + 3J(\omega_N) + 6J(\omega_H) + 6J(\omega_H + \omega_N)\}$$
$$+ (c^2/6)\{4J(0) + 3J(\omega_N)\} \qquad 2$$
$$\sigma_{NH} = (d^2/4)\{-J(\omega_H - \omega_N) + 6J(\omega_H + \omega_N)\} = R_1(NOE - 1)\gamma_N/\gamma_H$$

View Article Online
DOI: 10.1039/C5CP06197K

in which the dipolar coupling constant is $d = (\mu_0 h\gamma_H\gamma_N / 8\pi^2)r_{NH}^{-3}$, μ_0 is the permeability of free space, h is Planck's constant, r_{NH} is the average amide bond length (1.02 Å), the CSA coupling constant is $c = \Delta\sigma\omega_N/3^{1/2}$, $\Delta\sigma$ is the amide CSA (–172 ppm), ω_N and ω_H are the ^{15}N and ^{1}H frequencies at the respective static field, and $J(\omega)$ is the spectral density function. Using the reduced spectral density mapping approach, the above expressions can be converted to expressions for $J(0)$, $J(\omega_N)$ (at each static field) and $J(0.870\omega_H)$ (at each static field):

$$\begin{aligned} \Gamma_{auto} &= R_2 - 0.5R_1 - 0.454\sigma_{NH} = J(0)(3d^2 + 4c^2)/6 \\ J(\omega_N) &= \{R_1 - 1.249\sigma_{NH}\}/(3d^2/4 + c^2) \\ J(0.870\omega_H) &= 4\sigma_{NH}/(5d^2) \end{aligned} \quad 3$$

The value of $J(0)$ was obtained from the slope of a linear fit through the origin of Γ_{auto} vs. $(3d^2 + 4c^2)/6$ for all four static fields.

The most complex spectral density function consistent with the acquired data is an extended version of the Model-free spectral density function [57]:

$$J(\omega) = \frac{2}{5}\left\{\frac{S^2\tau_M}{1+\omega^2\tau_M^2} + \frac{(S_f^2 - S^2)\tau_s'}{1+\omega^2\tau_s'^2} + \frac{(1-S_f^2)\tau_f'}{1+\omega^2\tau_f'^2}\right\} \quad 4$$

in which S^2 is the square of the generalized order parameter and τ_M is the (effective) overall rotational correlation time for a given N-H bond vector. $S_s^2 = S^2/S_f^2$, and S_f^2 are the squares of the generalized order parameters for intramolecular motions with slow, τ_s, and fast, τ_f, correlation times, respectively. τ_s', and τ_f' are the inverse sums of the respective correlation time with τ_M: $\tau_s' = (1/\tau_M + 1/\tau_s)^{-1}$ and $\tau_f' = (1/\tau_M + 1/\tau_f)^{-1}$. This equation assumes that the stochastic processes governing τ_M, τ_s, and τ_f are statistically independent, which approximately

View Article Online
DOI: 10.1039/C5CP06197K

holds if the processes are time-scale separated ($\tau_M >> \tau_s >> \tau_f$). If $(0.870\omega_H\tau'_f)^2 \ll 1$ and $(\omega_N\tau'_s)^2 \gg 1$, then the spectral density function becomes a linear function of $(0.870\omega_H)^{-2}$ [58]:

$$J(0.870\omega_H) = m_H(0.870\omega_H)^{-2} + b_H \quad (5)$$

in which:

$$m_H = \frac{2}{5}\left\{S^2/\tau_M + (S_f^2 - S^2)/\tau'_s\right\}$$
$$b_H = \frac{2}{5}(1-S_f^2)\tau'_f \quad (6)$$

Similarly, if $(\omega_N\tau'_s)^2 \ll 1$ and $(\omega_N\tau_M)^2 \gg 1$, then the spectral density function becomes a linear function of ω_N^{-2}:

$$J(\omega_N) = m_N\omega_N^{-2} + b_N \quad (7)$$

in which:

$$m_N = \frac{2}{5}S^2/\tau_M$$
$$b_N = \frac{2}{5}\left\{(S_f^2 - S^2)\tau'_s + (1-S_f^2)\tau'_f\right\} \quad (8)$$

If the linear relationships hold for a given set of field-dependent relaxation measurements, then the values m_N, b_N, m_H, and b_H, together with

$$J(0) = \frac{2}{5}\left\{S^2\tau_M + (S_f^2 - S^2)\tau'_s + (1-S_f^2)\tau'_f\right\} \quad (9)$$

are sufficient to determine the five parameters in Equation 4:

View Article Online
DOI: 10.1039/C5CP06197K

$$S^2 = \frac{5}{2}\left[\{J(0) - b_N\} m_N\right]^{1/2}$$

$$\tau_M = \left[\{J(0) - b_N\} / m_N\right]^{1/2}$$

$$S_f^2 = S^2 + \frac{5}{2}\left[\{b_N - b_H\}\{m_H - m_N\}\right]^{1/2} \quad 10$$

$$\tau_f' = \frac{5}{2} b_H / (1 - S_f^2)$$

$$\tau_s' = \left[\{b_N - b_H\} / \{m_H - m_N\}\right]^{1/2}$$

Fitted slopes and intercepts in Equation 4 were determined by linear least squares regression, and errors in the Model-free parameters were propagated by Monte Carlo simulations.

Model-free analysis

Model-free analysis was performed with *relax* [53,54]. During analysis, relaxation parameters were entered in duplicate for each residue to account for the homodimeric structure of GCN4. In the first analysis, for comparison with spectral density mapping, an individual overall correlation time was fit for each residue (local τ_M). In the second analysis, for comparison with previous NMR [26] and molecular dynamics [30] results, fitting was performed first for residues located in or near the coiled-coil region (residues 25–58) using an individual correlation time for each residue (local τ_M). For residues located in or near the disordered region (residues 3–27 and 54–58), the correlation time was fixed to the average τ_M of the coiled-coil region, with the resulting χ^2 values being used to determine the classification of residues located at the interface of the disordered and ordered regions (25—27 and 54—58). Parameters of the following models, enumerated in the *relax* documentation, were fit to the data:

View Article Online
DOI: 10.1039/C5CP06197K

$$\text{Model 0:}\quad J(\omega)=\frac{2}{5}\tau_m$$

$$\text{Model 1:}\quad J(\omega)=\frac{2}{5}\tau_m\left[\frac{S^2}{1+(\omega\tau_m)^2}\right]$$

$$\text{Model 2:}\quad J(\omega)=\frac{2}{5}\tau_m\left[\frac{S^2}{1+(\omega\tau_m)^2}+\frac{(1-S^2)(\tau_e+\tau_m)\tau_e}{(\tau_e+\tau_m)^2+(\omega\tau_e\tau_m)^2}\right] \qquad 11$$

$$\text{Model 5:}\quad J(\omega)=\frac{2}{5}\tau_m\left[\frac{S^2}{1+(\omega\tau_m)^2}+\frac{(S_f^2-S^2)(\tau_s+\tau_m)\tau_s}{(\tau_s+\tau_m)^2+(\omega\tau_s\tau_m)^2}\right]$$

$$\text{Model 6:}\quad J(\omega)=\frac{2}{5}\tau_m\left[\frac{S^2}{1+(\omega\tau_m)^2}+\frac{(1-S_f^2)(\tau_f+\tau_m)\tau_f}{(\tau_f+\tau_m)^2+(\omega\tau_f\tau_m)^2}+\frac{(S_f^2-S^2)(\tau_s+\tau_m)\tau_s}{(\tau_s+\tau_m)^2+(\omega\tau_s\tau_m)^2}\right]$$

Model-free analysis was performed using only models that lack contribution from conformational exchange (0, 1, 2, 5, and 6, Equation 11) [21,22,57]. Best fit models were selected using the Bayesian Information Criterion (BIC) [59]. Errors for the Model-free parameters were determined from 500 Monte Carlo simulations.

Results

Assignment of GCN4 amide resonances

The assignment of U-[^{15}N, ^{2}H] GCN4 chemical shifts utilized a ^{1}H,^{15}N,^{15}N HSQC-NOESY-HSQC with 600 ms mixing time [60]. In the coiled-coil region, NOE connectivities were observed for residues ranging from i_{-3} to i_{+3} (Figure S1A), whereas connectivities for i_{-2} to i_{+2} were generally observed in the disordered basic region (Figure S1B). The amide chemical shift assignments are listed in Table S2. The exclusive use of amides for resonance assignments is advantageous because an additional ^{13}C-labeled sample is not required and because the indirect dimensions can be acquired with very high resolution due to the narrow ^{15}N chemical shift range and the absence of constant-time pulse sequence elements. In the case of GCN4, this strategy also enabled resonance assignment and spin relaxation experiments to be conducted on

View Article Online
DOI: 10.1039/C5CP06197K

the same sample. Amide chemical shift assignments (Figure S2 and Table S2) were further confirmed using those reported by Bracken, *et. al* [26] and with an HNCA and HN(CO)CA collected on U-[^{15}N, ^{13}C] GCN4 (data not shown).

Fast timescale dynamics of GCN4

Established amide spin relaxation experiments were performed to measure the ^{15}N R_1, ^{15}N R_2, and {^{1}H}-^{15}N heteronuclear NOE spin relaxation rate constants of U-[^{15}N, ^{2}H] GCN4 (Table S3) at four static fields (14.1, 16.45, 18.8, and 21.1 T). The structurally heterogeneous nature of GCN4 leads to significantly different peak intensities in the disordered and coiled-coil regions, creating additional considerations for the acquisition and analysis of quantitative NMR experiments. An increased number of t_1 increments and additional relaxation time points were collected to ensure accurate digitization. To ensure accurate error estimation during Monte Carlo analysis, residues were analyzed in two groups based on initial peak intensities. The relaxation rate constants are consistent with a disordered basic region, having elevated R_1 relaxation rates, reduced R_2 relaxation rates, and reduced heteronuclear NOE values, relative to those of the coiled-coil region (Figure 2).

Plots of Γ_{auto} vs. $(3d^2 + 4c^2)/6$, $J(\omega_N)$ vs. ω_N^{-2}, and $J(0.870\omega_H)$ vs. $(0.870\omega_H)^{-2}$ were well-fit by the linear equations 3, 5, and 7, respectively. Examples of the fitted data are shown in Figure 3A–C for residue 14. The excellent fits of Γ_{auto} vs. $(3d^2 +4c^2)/6$ for the assumed value of $\Delta\sigma = -172$ ppm indicate chemical exchange does not contribute significantly to the measured R_2 values. The absence of exchange contributions was also confirmed by comparing fits of Γ_{auto} vs. B_0^2 performed with $R_{ex} = 0$ and with R_{ex} as a fitted parameter, which was assumed to scale with B_0^2 (data not shown). The linearity of the graphs of these three sets of data implies that only five

View Article Online
DOI: 10.1039/C5CP06197K

independent parameters are needed to describe the data and therefore Equation 4 is the most complex spectral density function supported. Motions may be distributed over multiple time scales so that τ_M, τ_s, and τ_e represent effective fits to a more complex distribution of correlation times.

Reduced spectral density analysis of GCN4

The values of $S^2\tau_M$, S^2/τ_M, $(S_f^2 - S^2)\tau_s'$, $(S_f^2 - S^2)/\tau_s'$, and $(S_f^2 - S^2)\tau_s'$ obtained from Equations 6, 8, and 9 are shown in Figure 4A–E. The lack of mobility for the coiled coil and the extensive mobility of the basic region are evident directly from these plots. Figure 4F plots $(S_f^2 - S^2)\tau_s'$ vs. $S^2\tau_M$, showing that four clusters of residues with related properties are evident: 3–12 (pink), 13–25 (green), 26–55 (black), and 56–58 (orange). The values of the Model-free parameters determined from the data in Figure 4 using Equation 10 are shown in Figure 5; values of τ_f and τ_s with extremely large uncertainties, because the corresponding S_f^2 or S_s^2 approaches unity, are not displayed for clarity. To test the accuracy of the assumptions used to obtain the Model-free parameters from the above equations, the relaxation data also were analyzed conventionally using the program *relax* and assuming a local τ_M for each residue. Figure 3D shows fitted spectral density values for residue 14 determined from the spectral density mapping and conventional analyses. Figure 6 compares $S^2\tau_M$, S^2, and τ_M for all residues using the two analyses.

Model-free analysis of GCN4

Treatment of the basic region, coiled coil, and C-terminal region during Model-free analysis of GCN4 was similar to the method used by Bracken and coworkers [26]. Briefly, the

View Article Online
DOI: 10.1039/C5CP06197K

coiled-coil residues were first analyzed using a local correlation time (τ_M), and then the mean τ_M from this analysis was fixed for the basic region. The fitted Model-free parameters for residues in the coiled-coil incorporate the effects of diffusion anisotropy through the local τ_M values. Based on the modest diffusion tensor anisotropy $2D_{zz}/(D_{xx}+D_{yy}) = 1.25$ determined from the local τ_M for residues in the coiled-coil region, further treatment of the global diffusion tensor is unlikely to significantly effect results for the residues in the basic region: a root-mean-square error of ~4% in S2 would arise from different (unknown) average orientations of N-H bond vectors for these residues [61]. In the current study, a more detailed analysis, including the fitting of internal correlation times, was possible using spin relaxation data acquired at multiple static fields. Three of the models were originally described by Lipari and Szabo [21,22] and have Brownian rotational diffusion characterized by a correlation time (τ_M) and the following dynamic properties: no dynamics (model 0), internal motion that can be characterized by a single order parameter (S^2, model 1), or an order parameter plus an effective internal correlation time (τ_e, model 2). When $\tau_e < 100$ ps, the internal motion was classified as fast (τ_f), otherwise it was slow (τ_s). Two additional models (5 and 6) developed by Clore, *et. al* [57] include internal motions on two timescales, the faster of which is described by τ_f and S_f^2 and the slower by τ_s and S_s^2, which are determined as described above. Given the lack of evidence for chemical exchange, as determined by analysis of Γ_{auto}, additional models containing an R_{ex} term were not considered.

The selected model, as determined by the Bayesian information criterion (BIC) [59], is shown for reach residue in Table S4. Models 2 and 5 were chosen for the coiled-coil region indicating simpler dynamics, while model 6 was chosen for all of the disordered residues. The model selected for the disordered residues does not change in most cases when a local τ_M was

View Article Online
DOI: 10.1039/C5CP06197K

assumed (see above) indicating the selection of a more complicated model in this region is not merely reflective of the reduced degree of freedom. The χ^2 values (Table S4) observed for the basic region are slightly higher than those of the coiled-coil region, but considerably less than those observed for the extreme N- and C-terminal residues. Based on the lowest χ^2 value from analyses where τ_M was either fit as a parameter or held constant, residues at the ordered-disordered interface were classified as follows: residues 26, 27, and 54 were considered part of the coiled-coil region while residues 25 and 55—58 were considered disordered.

The resulting Model-free parameters are plotted in Figure 7. The trends in parameters are similar to those obtained in the current study from reduced spectral density mapping (Figure 5), although the order parameters in the basic region are reduced because the global value of τ_M assumed in Model-free analysis (16.9 ns) is larger than the local overall correlation times determined by reduced spectral density mapping. The order parameter (S^2) has a mean value of 0.91 for the coiled-coil region (Table S4 and Figure 7A) and the value of this parameter decreases gradually along the basic region.

The acquisition of relaxation parameters at multiple static fields enables the study of multiple (fast and/or slow) internal motions [57]. The basic region of GCN4 has a fast internal process (Table S4 and Figure 7F) with a correlation time $\tau_f \approx 40–70$ ps. There is also evidence for motions with correlation times in this range in the coiled-coil region, although the uncertainty on these values is much greater. The motions that dominate the internal order parameter for the basic region actually have a slower correlation time, as shown in Figure 7C by the lower values of S_s^2 (lower order parameters imply a larger degree of conformational variability), relative to the higher values of S_f^2 (Figure 7E). These slower internal motions have a correlation time $\tau_s \approx 1.4–2.5$ ns (Figure 7D).

View Article Online
DOI: 10.1039/C5CP06197K

Discussion

Comparison of spectral density and Model-free analysis results

The Model-free parameters determined from spectral density mapping bear a strong similarity to those determined from full analysis with *relax* (Figure S3). The order parameters (S^2, Figures 5A, 7A, and S3A) are large in the coiled-coil region and decrease dramatically in the basic region toward the N-terminus. The values of S^2 in the basic region are somewhat larger if local overall correlation times are assumed in the model spectral density function, compared to values obtained when the overall rotational correlation time is fixed at the mean value for the coiled-coil domain. This reflects different averaging of effective correlation times in the two analyses. Strikingly, S_f^2 decreases to a plateau value (~0.6 in Figures 7E and S3E), while S_s^2 decreases dramatically to very low values at the N-terminus (Figures 7C and S3C). Values of S_f^2 (and consequently S^2) are elevated around residues 14–20 and, to a slightly lesser extent, residues 5–9, although the overall magnitude is reduced when τ_M was fixed (Figures 5E, 7E, and S3E). The presence of such local regions of elevated order parameters independent of calculation method indicates they likely adopt transiently ordered conformations. The effective internal correlation times for residues in the basic region have narrow distributions, with average values of τ_f = 48.9 ps and τ_s = 1.6 ns for the analysis with fixed τ_M. (Again, the same qualitative behavior is observed if local overall correlation times are utilized, albeit with somewhat different correlation times.) The local correlation times (τ_M) determined from spectral density calculations and full Model-free analysis also are nearly identical in the coiled-coil region (Figures 5B, 7B, and S3B). These findings demonstrate that spectral density mapping using at least three static magnetic fields can generate effective local correlation times in the

View Article Online
DOI: 10.1039/C5CP06197K

absence of assumptions about a global τ_M, thus demonstrating the feasibility of using Model-free analysis to study IDPs in some cases.

Consistency with previous studies of GCN4 dynamics

The τ_M of the coiled-coil residues determined by Model-free analysis has a mean value of 16.9 ns (Figure 7B). This value is lower than that determined previously [26] (mean τ_M = 18.9 ns), which is likely due to transient aggregation at the higher sample concentration used in the earlier study [26]. In both this and the previous study, determination of dynamical parameters for the disordered region is enabled by the assumption that a single τ_M dominates global motions. Though the dynamics of intrinsically disordered proteins is a topic of ongoing study, molecular dynamics simulations do support this assumption [30,62].

The Model-free derived order parameters determined using a fixed overall correlation time for the basic region (Figure 8, black) are in excellent agreement with those determined previously by NMR at a single static magnetic field of 11.7 T [26] (Pearson's r = 0.997 and Figure 8, blue) and by Robustelli, *et. al* [27] (see trajectory 2, Figure 4 in the reference) using molecular dynamics simulations (r = 0.982 and Figure 8, orange). In particular, elevated order parameters are noted for two parts of the disordered region, referred to as helix 1 (H1, residues A5–R9) and helix 2 (H2, residues Q14–R20), believed to form transient helices which may help pre-order this region for binding of DNA substrate [30]. Similar elevations are observed for the multi-field NMR data, particularly for H2 (Figure 8 and Table S4).

View Article Online
DOI: 10.1039/C5CP06197K

Biological implications of structural fluctuations and dynamical rates

The binding of GCN4 to DNA requires the formation of the basic region helices that insert into the DNA major groove, potentially incurring a large entropic cost. The magnitude of this penalty is considerably reduced by the presence of helix-capping sequences, such as the one prior to H1, which nucleate transient helix formation [63]. The observed regions of elevated order parameters (H1 and H2), which are corroborated by previous NMR [26] and molecular dynamics [30] studies, are consistent with the formation of these structures. Estimates of conformational entropy derived from S^2 are generally consistent with estimates of conformational entropy derived from calorimetric measurements [26].

The existence of such transient helices may also enable GCN4 to bind DNA with on-rates at or near that of the diffusion limit (~10^{10} $M^{-1}s^{-1}$ [64]) by pre-organizing the DNA binding domain. The correlation time of slow internal motions (τ_s) ranges between 1.4 and 2.5 ns, which is faster than both the binding rate of GCN4 to DNA (k_{on} ~10^6–10^{10} $M^{-1}s^{-1}$ [65,66], which gives k_{on}[DNA] ~10^2 s^{-1}, assuming μM ligand concentration) and the off rate (~10^5–10^6 s^{-1} [67,68]). Thus, these large amplitude motions could facilitate formation and rearrangement of transient encounter complexes to yield the well-ordered protein-DNA complex structure. Collectively, these observations lend further evidence to the combined and subsequent roles of conformational selection and induced fit in GCN4 binding to DNA and for IDP target recognition, in general.

View Article Online
DOI: 10.1039/C5CP06197K

Conclusions

We have measured the backbone ^{15}N spin relaxation rate constants of *apo* GCN4 bZip DNA-binding domain at four static magnetic fields and demonstrated that both reduced spectral density mapping and the Model-free formalism can be used to analyze the dynamics of an intrinsically disordered region. The order parameters (S^2) obtained from Model-free analysis are highly similar to those obtained from spectral density mapping of GCN4 at a single static field [26] and to molecular dynamics simulations [30], while the internal dynamics parameters determined in the current study provide additional insight. Local regions with elevated order parameters in the basic region [26,30] are consistent with structural pre-organization of nascent helices prior to binding of DNA substrate. Additionally, we are able to determine the internal correlation times for conformational dynamics of the basic region and find that the basic region undergoes large amplitude internal motions whose correlation time ($\tau_s \approx 1.4–2.5$ ns) would allow induced formation of the fully helical basic region within the lifetime of a protein-DNA encounter complex. Thus, binding of the GCN4 bZip domain to DNA involves the, possibly correlated, steps of selected-fit and induced-fit interactions.

Acknowledgements

A.G.P. and M.L.G acknowledge support from National Institute of Health grants GM50291 and GM089047, respectively. The AVANCE 600 NMR spectrometer at Columbia University was purchased with the support of NIH grant RR026540. A.G.P. is a member of the New York Structural Biology Center (NYSBC). The data acquired at 16.45, 18.8 and 21.1 T were collected at NYSBC, which was made possible by a NYSTAR grant and ORIP/NIH facility improvement grant CO6RR015495. The 900 MHz NMR spectrometers were purchased with funds from NIH

View Article Online
DOI: 10.1039/C5CP06197K

grant P41GM066354, the Keck Foundation, New York State Assembly, and U.S. Department of Defense. This research was partially supported by the Intramural Research Program of the National Cancer Institute.

View Article Online
DOI: 10.1039/C5CP06197K

References

1. A. K. Dunker, C. J. Brown, J. D. Lawson, L. M. Iakoucheva and Z. Obradović, *Biochemistry,* 2002, **41,** 6573-6582.

2. P. E. Wright and H. J. Dyson, *J. Mol. Biol.,* 1999, **293,** 321-331.

3. V. N. Uversky, *Protein Sci.,* 2002, **11,** 739-756.

4. P. Tompa, N. E. Davey, T. J. Gibson and M. M. Babu, *Mol. Cell,* 2014, **55,** 161-169.

5. L. M. Iakoucheva, C. J. Brown, J. D. Lawson, Z. Obradović and A. K. Dunker, *J. Mol. Biol.,* 2002, **323,** 573-584.

6. P. E. Wright and H. J. Dyson, *Nat. Rev. Mol. Cell Biol.,* 2014, **16,** 18-29.

7. C. A. Galea, Y. Wang, S. G. Sivakolundu and R. W. Kriwacki, *Biochemistry,* 2008, **47,** 7598-7609.

8. J. Liu, N. B. Perumal, C. J. Oldfield, E. W. Su, V. N. Uversky and A. K. Dunker, *Biochemistry,* 2006, **45,** 6873-6888.

9. K. Sugase, H. J. Dyson and P. E. Wright, *Nature,* 2007, **447,** 1021-1025.

10. T. Mittag and J. D. Forman-Kay, *Curr. Opin. Struct. Biol.,* 2007, **17,** 3-14.

11. M. Fuxreiter, I. Simon, P. Friedrich and P. Tompa, *J. Mol. Biol.,* 2004, **338,** 1015-1026.

12. J. R. Williamson, *Nat. Struct. Biol.,* 2000, **7,** 834-837.

View Article Online
DOI: 10.1039/C5CP06197K

13. V. Z. Miloushev, F. Bahna, C. Ciatto, G. Ahlsen, B. Honig, L. Shapiro and A. G. Palmer, *Structure,* 2008, **16,** 1195-1205.

14. G. G. Hammes, Y. C. Chang and T. G. Oas, *Proc. Natl. Acad. Sci. U. S. A.,* 2009, **106,** 13737-13741.

15. Q. Wang, P. Zhang, L. Hoffman, S. Tripathi, D. Homouz, Y. Liu, M. N. Waxham and M. S. Cheung, *Proc. Natl. Acad. Sci. U. S. A.,* 2013, **110,** 20545-20550.

16. J. Dogan, T. Schmidt, X. Mu, Engström and P. Jemth, *J. Biol. Chem.,* 2012, **287,** 34316-34324.

17. C. J. Oldfield, Y. Cheng, M. S. Cortese, P. Romero, V. N. Uversky and A. K. Dunker, *Biochemistry,* 2005, **44,** 12454-12470.

18. H. J. Dyson and P. E. Wright, *Nat. Rev. Mol. Cell Biol.,* 2005, **6,** 197-208.

19. H. J. Dyson and P. E. Wright, *Methods Enzymol.,* 2001, **339,** 258-270.

20. S. Cavagnero, C. Nishimura, S. Schwarzinger, H. J. Dyson and P. E. Wright, *Biochemistry,* 2001, **40,** 14459-14467.

21. G. Lipari and A. Szabo, *J. Am. Chem. Soc.,* 1982, **104,** 4546-4559.

22. G. Lipari and A. Szabo, *J. Am. Chem. Soc.,* 1982, **104,** 4559-4570.

23. M. Miller, *Curr. Protein Pept. Sci.,* 2009, **10,** 244-269.

24. T. E. Ellenberger, C. J. Brandl, K. Struhl and S. C. Harrison, *Cell,* 1992, **71,** 1223-1237.

View Article Online
DOI: 10.1039/C5CP06197K

25. V. Saudek, A. Pastore, M. A. Morelli, R. Frank, H. Gausepohl and T. Gibson, *Protein Eng.,* 1991, **4,** 519-529.

26. C. Bracken, P. A. Carr, J. Cavanagh and A. G. Palmer, *J. Mol. Biol.,* 1999, **285,** 2133-2146.

27. M. A. Weiss, T. Ellenberger, C. R. Wobbe, J. P. Lee, S. C. Harrison and K. Struhl, *Nature,* 1990, **347,** 575-578.

28. V. Saudek, A. Pastore, M. A. Castiglione Morelli, R. Frank, H. Gausepohl, T. Gibson, F. Weih and P. Roesch, *Protein Eng.,* 1990, **4,** 3-10.

29. V. Saudek, H. S. Pasley, T. Gibson, H. Gausepohl, R. Frank and A. Pastore, *Biochemistry,* 1991, **30,** 1310-1317.

30. P. Robustelli, N. Trbovic, R. A. Friesner and A. G. Palmer, *J. Chem. Theory Comput.,* 2013, **9,** 5190-5200.

31. M. Findeisen, T. Brand and S. Berger, *Magn. Reson. Chem.,* 2007, **45,** 175-178.

32. S. Grzesiek and A. Bax, *J. Magn. Reson. (1969),* 1992, **96,** 432-440.

33. J. Schleucher, M. Sattler and C. Griesinger, *Angew. Chem. Int. Edit.,* 1993, **32,** 1489-1491.

34. L. E. Kay, G. Y. Xu and T. Yamazaki, *J. Magn. Reson. A,* 1994, **109,** 129-133.

35. M. Ikura, A. Bax, G. M. Clore and A. M. Gronenborn, *J. Am. Chem. Soc.,* 1990, **112,** 9020-9022.

36. T. Diercks, M. Coles and H. Kessler, *J. Biomol. NMR,* 1999, **15,** 177-180.

View Article Online
DOI: 10.1039/C5CP06197K

37. J. Skelton, G. Palmer, M. Akke, J. Kordel, M. Rance and J. Chazin, *J. Magn. Reson. B,* 1993, **102,** 253-264.

38. N. A. Farrow, O. Zhang, J. D. Forman-Kay and L. E. Kay, *Biochemistry,* 1995, **34,** 868-878.

39. G. N. Yip and E. R. Zuiderweg, *J. Magn. Reson.,* 2004, **171,** 25-36.

40. J. Cavanagh, A. G. Palmer, P. E. Wright and M. Rance, *J. Magn. Reson. (1969),* 1991, **91,** 429-436.

41. A. G. Palmer, M. Rance and P. E. Wright, *J. Am. Chem. Soc.,* 1991, **113,** 4371-4380.

42. A. G. Palmer, J. Cavanagh, R. A. Byrd and M. Rance, *J. Magn. Reson. (1969),* 1992, **96,** 416-424.

43. L. Kay, P. Keifer and T. Saarinen, *J. Am. Chem. Soc.,* 1992, **114,** 10663-10665.

44. F. Delaglio, S. Grzesiek, G. W. Vuister, G. Zhu, J. Pfeifer and A. Bax, *J. Biomol. NMR,* 1995, **6,** 277-293.

45. T. Goddard and D. G. Kneller, *SPARKY 3,* University of California, San Francisco.

46. S. V. van der Walt, S. C. Colbert and G. V. Varoquaux, *Comput. Sci. Eng.,* 2011, **13,** 22-30.

47. K. J. Millman and M. Aivazis, *Comput. Sci. Eng.,* 2011, **13,** 9-12.

48. T. E. Oliphant, *Comput. Sci. Eng.,* 2007, **9,** 10-20.

49. J. D. Hunter, *Comput. Sci. Eng.,* 2007, **9,** 90-95.

50. F. Pérez and B. E. Granger, *Comput. Sci. Eng.,* 2007, **9,** 21-29.

View Article Online
DOI: 10.1039/C5CP06197K

51. W. McKinney, *Proceedings of the 9th Python in Science Conference,* 2010, 51-56.

52. J. J. Helmus and C. P. Jaroniec, *J. Biomol. NMR,* 2013, **55,** 355-367.

53. E. d'Auvergne and P. Gooley, *J. Biomol. NMR,* 2008, **40,** 107-119.

54. E. d'Auvergne and P. Gooley, *J. Biomol. NMR,* 2008, **40,** 121-133.

55. R. Bruschweiler, X. Liao and P. Wright, *Science,* 1995, **268,** 886-889.

56. L. K. Lee, M. Rance, W. J. Chazin and A. G. Palmer, *J. Biomol. NMR,* 1997, **9,** 287-298.

57. G. M. Clore, A. Szabo, A. Bax, L. E. Kay, P. C. Driscoll and A. M. Gronenborn, *J. Am. Chem. Soc.,* 1990, **112,** 4989-4991.

58. K. H. Mayo, V. A. Daragan, D. Idiyatullin and I. Nesmelova, *J. Magn. Reson.,* 2000, **146,** 188-195.

59. E. d'Auvergne and P. Gooley, *J. Biomol. NMR,* 2003, **25,** 25-39.

60. O. Zhang, J. D. Forman-Kay, D. Shortle and L. E. Kay, *J. Biomol. NMR,* 1997, **9,** 181-200.

61. M. L. Gill and A. G. Palmer, *J. Phys. Chem. B,* 2014, **118,** 11120-11128.

62. Y. Xue and N. R. Skrynnikov, *J. Am. Chem. Soc.,* 2011, **133,** 14614-14628.

63. J. J. Hollenbeck, D. L. McClain and M. G. Oakley, *Protein Sci.,* 2002, **11,** 2740-2747.

64. R. A. Alberty and G. G. Hammes, *J. Phys. Chem.,* 1958, **62,** 154-159.

View Article Online
DOI: 10.1039/C5CP06197K

65. J. J. Kohler, S. J. Metallo, T. L. Schneider and A. Schepartz, *Proc. Natl. Acad. Sci. U. S. A.,* 1999, **96,** 11735-11739.

66. S. E. Halford and J. F. Marko, *Nucleic Acids Res.,* 2004, **32,** 3040-3052.

67. Y. Okahata, K. Niikura, Y. Sugiura, M. Sawada and T. Morii, *Biochemistry,* 1998, **37,** 5666-5672.

68. J. J. Kohler and A. Schepartz, *Biochemistry,* 2001, **40,** 130-142.

View Article Online
DOI: 10.1039/C5CP06197K

Figure Captions

Figure 1. (**A**) The bZip region of GCN4 contains a C-terminal coiled-coil region (blue) that forms a leucine zipper, while the N-terminal basic region (red) interacts with DNA substrate (gray). Crystallographic coordinates are from PDB 1YSA [24]. (**B**) The inverse of the order parameters (S^2) determined by Bracken and coworkers [26] are mapped onto the width and color of the bZip domain. Narrow regions that are colored blue are the most rigid (highest S^2), while wider regions that are colored red are the most dynamic (lowest S^2).

Figure 2. Relaxation measurements for (**A**) R_1, (**B**) R_2, and (**C**) $\{^1H\}$-^{15}N heteronuclear NOE experiments performed on GCN4. Data for 14.1, 16.45, 18.8, and 21.1 T are black, blue, orange, and green, respectively. Error bars are the result of Monte Carlo simulations for the R_1 and R_2 measurements and based on the noise floor for the heteronuclear NOE.

Figure 3. Spectral density mapping for residue 14 of the GCN4 bZip domain. (**A**) Γ_{auto} at 14.1, 16.45, 18.8, and 21.1 T plotted vs. $(3d^2 + 4c^2)/6$ (Equation 3). The solid line is the best fit through the origin to determine J(0) from the slope. (**B**) $J(\omega_N)$ and (**C**) $J(0.870\omega_H)$ are plotted vs. ω^{-2}. Solid lines are the best linear fits to the data. (**D**) Reduced spectral density values $J(\omega)$ plotted vs. ω. The solid line is determined from the Model-free parameters obtained from the spectral density mapping protocol (Equation 10); the dashed line is calculated from Model-free parameters determined from full analysis using the relax program assuming a local overall rotational correlation time τ_M for each residue.

View Article Online
DOI: 10.1039/C5CP06197K

Figure 4. Aggregate Model-free parameters from field-dependent spectral density mapping. The values of (**A**) $S^2\tau_M$, (**B**) S^2/τ_M, (**C**) $(S_f^2 - S^2)\tau_s'$, (**D**) $(S_f^2 - S^2)/\tau_s'$, and (**E**) $(S_f^2 - S^2)\tau_s'$ obtained from Equations 6–9 are shown. (**F**) $(S_f^2 - S^2)\tau_s'$ is plotted vs. $S^2\tau_M$. Regions of the protein are colored as follows: region 1 on bZip (residues 3–12): pink; region 2 of bZip (residues 13–25): green; coiled-coil (residues 26–55): black; disordered C-term (residues 56–58): orange.

Figure 5. Model-free parameters from field-dependent spectral density mapping. Values of (**A**) S^2, (**B**) τ_M, (**C**) S_s^2, (**D**) τ_s, (**E**) S_f^2, and (**F**) τ_f are plotted vs. residue number. Values not statistically different from zero are not shown. Colors are as in Figure 4.

Figure 6. Comparison of Model-free parameters (**A**) $S^2\tau_M$, (**B**) S^2, and (**C**) τ_M from field-dependent spectral density mapping and the full analysis in which local τ_M values were fit using the relax program. The correlation coefficients are 0.999, 0.964, and 0.964, respectively. Colors are as in Figure 4.

Figure 7. Model-free from field-dependent analysis using full analysis with relax. Values of (**A**) S^2, (**B**) τ_M, (**C**) S_s^2, (**D**) τ_s, (**E**) S_f^2, and (**F**) τ_f are plotted vs. residue number. Overall correlation times (τ_M) were determined individually for residues in the coiled-coil region. τ_M was fixed at 16.9 ns for residues in the basic region and C-terminal residues, as denoted by the horizontal line in (B). Colors are as in Figure 4.

Figure 8. Comparison of order parameters (S^2) for GCN4 as determined in the current study (black) to those determined by previously at a single static field of 11.7 T by Bracken, *et. al* [26]

View Article Online
DOI: 10.1039/C5CP06197K

(blue) and by Robustelli, *et al.* [30] (orange) using a series of 100 ns molecular dynamics simulations.

View Article Online
DOI: 10.1039/C5CP06197K

Figure 1

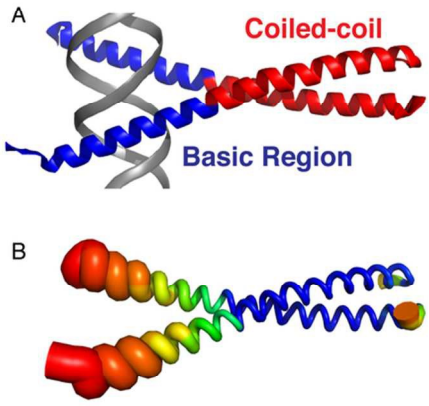

85x46mm (300 x 300 DPI)

View Article Online
DOI: 10.1039/C5CP06197K

Figure 2

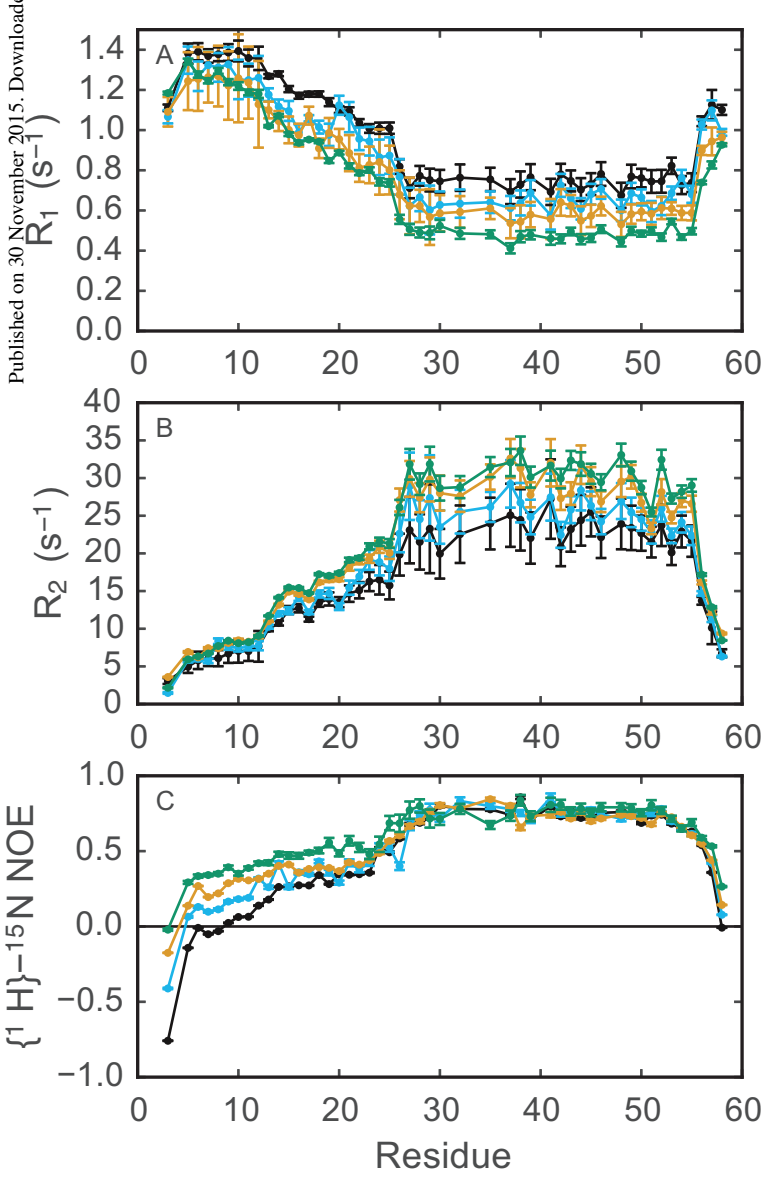

View Article Online
DOI: 10.1039/C5CP06197K

Figure 3

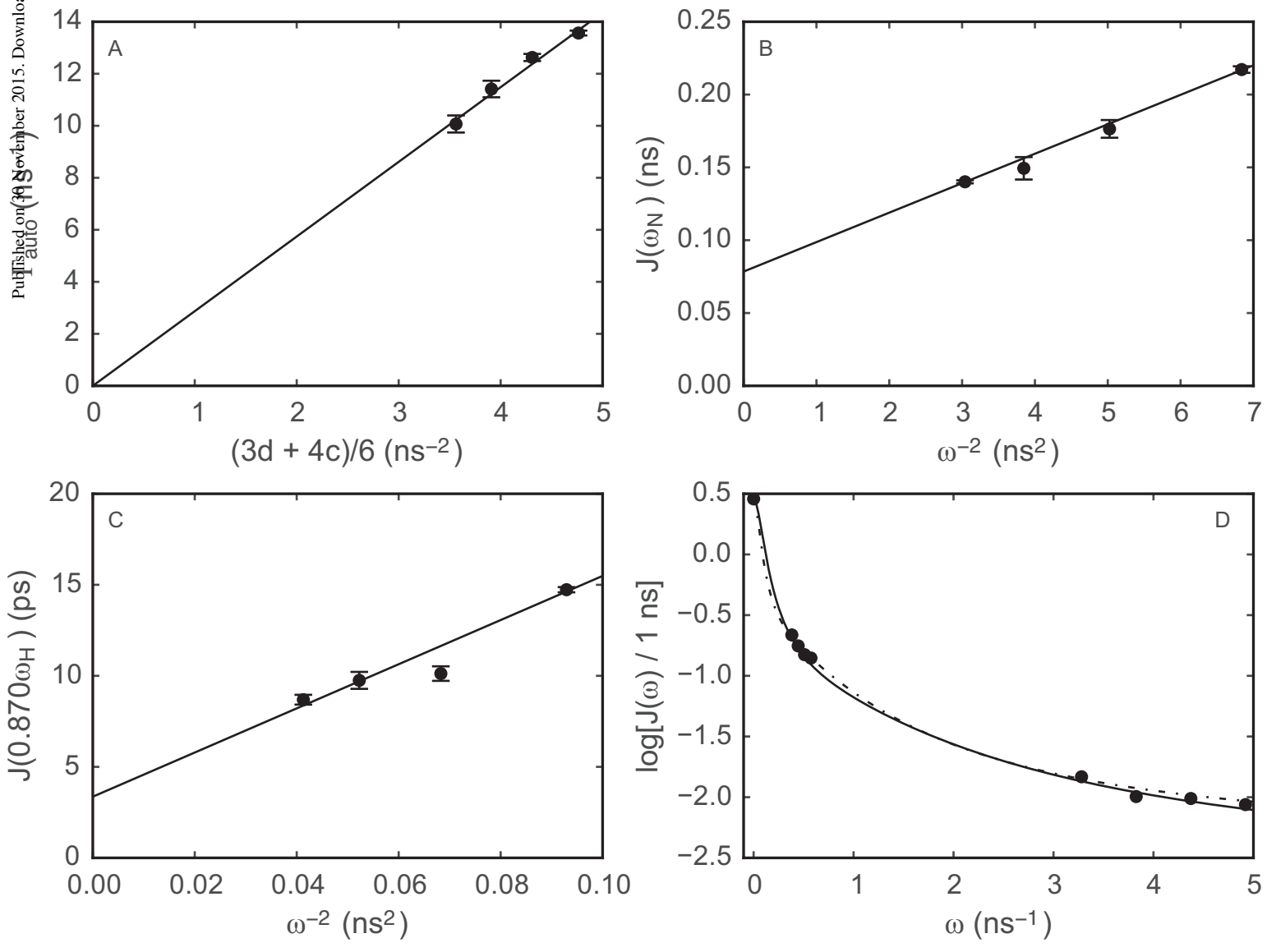

View Article Online
DOI: 10.1039/C5CP06197K

Figure 4

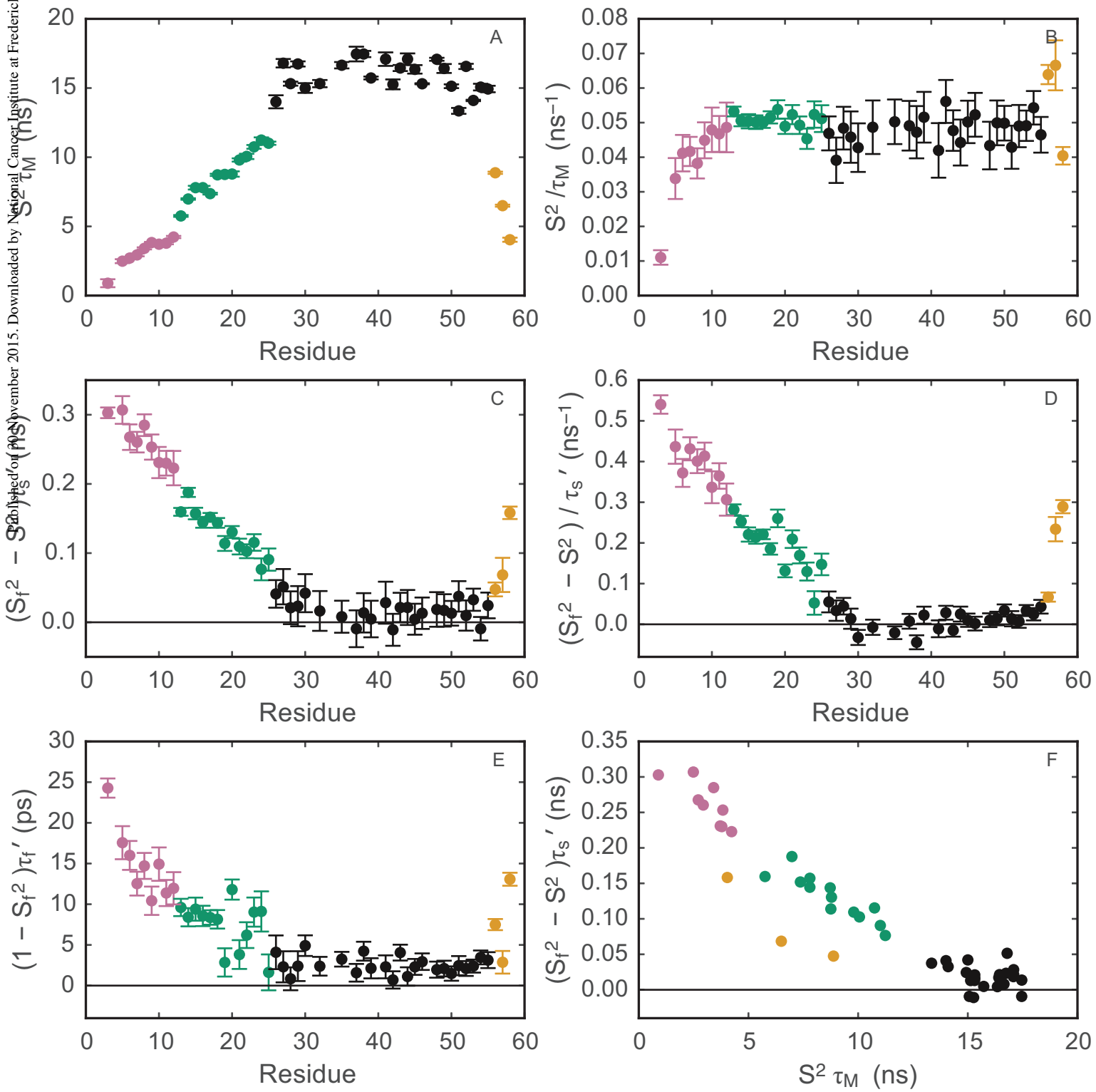

View Article Online
DOI: 10.1039/C5CP06197K

Figure 5

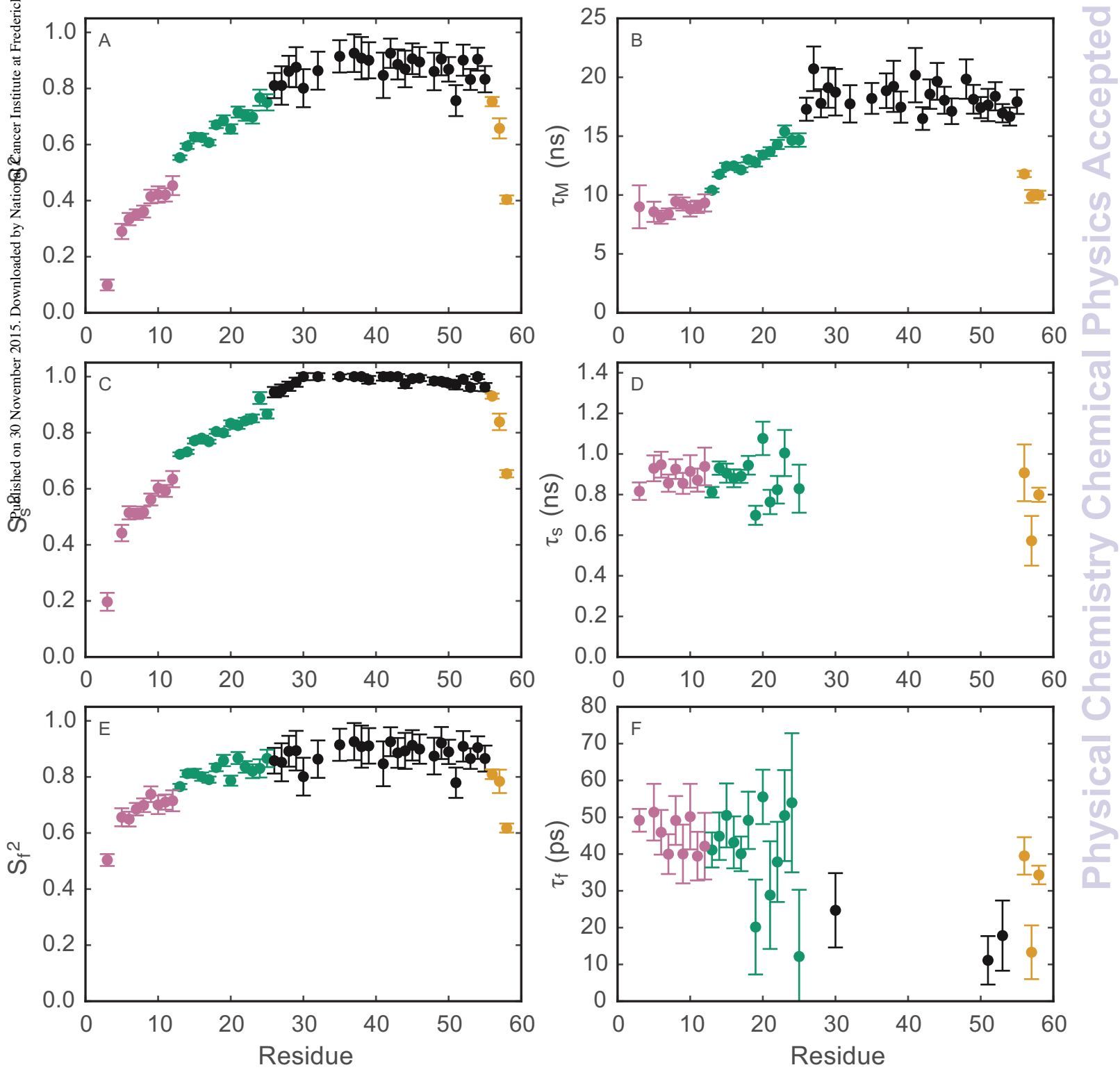

View Article Online
DOI: 10.1039/C5CP06197K

Figure 6

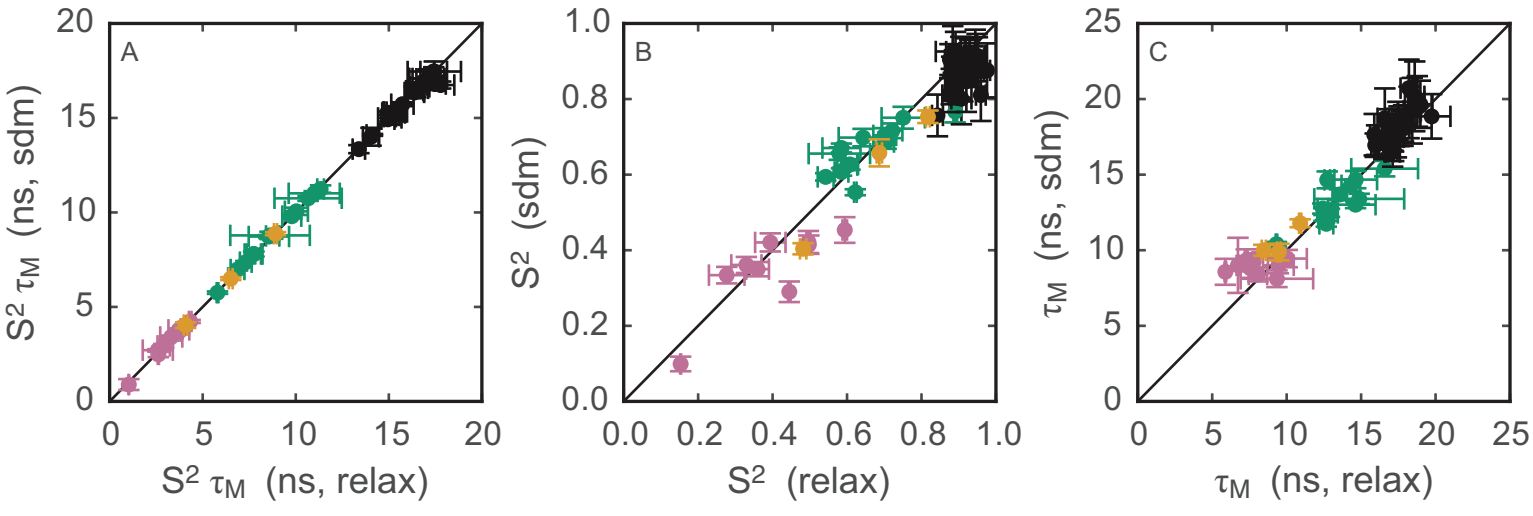

View Article Online
DOI: 10.1039/C5CP06197K

Figure 7

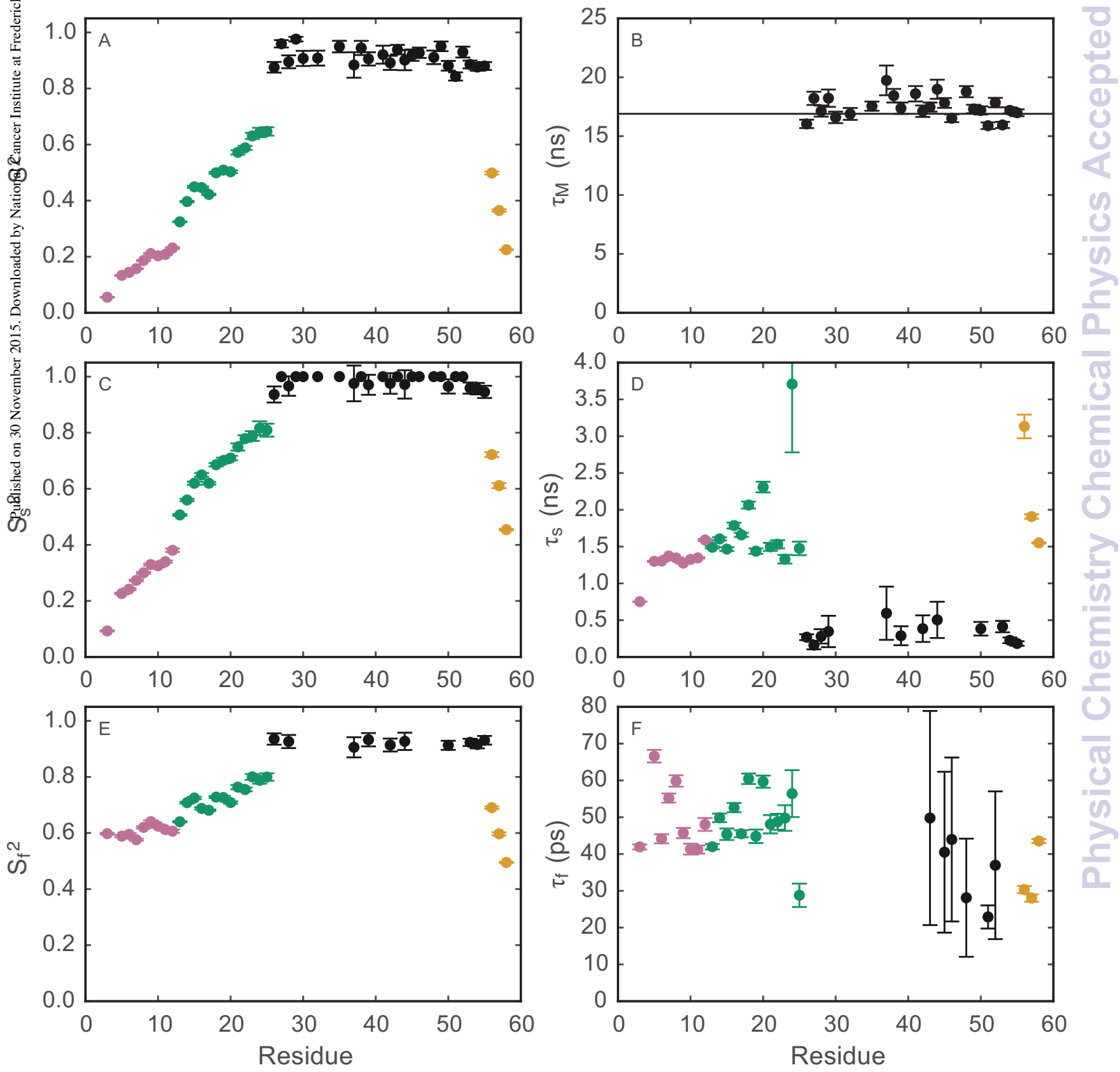

View Article Online
DOI: 10.1039/C5CP06197K

Figure 8

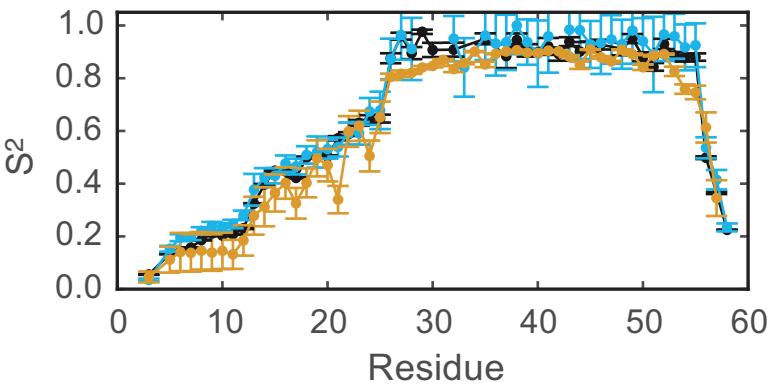

Electronic Supplementary Material (ESI) for Physical Chemistry Chemical Physics.

Supplemental Figures and Tables

Dynamics of GCN4 Facilitate DNA Interaction: A Model-Free Analysis of an Intrinsically Disordered Region

Michelle L. Gill,[1,2] R. Andrew Byrd,[2] and Arthur G. Palmer, III[1*]

[1]Department of Biochemistry and Molecular Biophysics
Columbia University
New York, NY 10032

[2]Structural Biophysics Laboratory
National Cancer Institute
National Institutes of Health
Frederick, MD 21702

[*]Address correspondence to:
Arthur G. Palmer, III
Tel: (212) 305-8675
Fax: (212) 305-7932
Email: agp6@columbia.edu

Figure S1

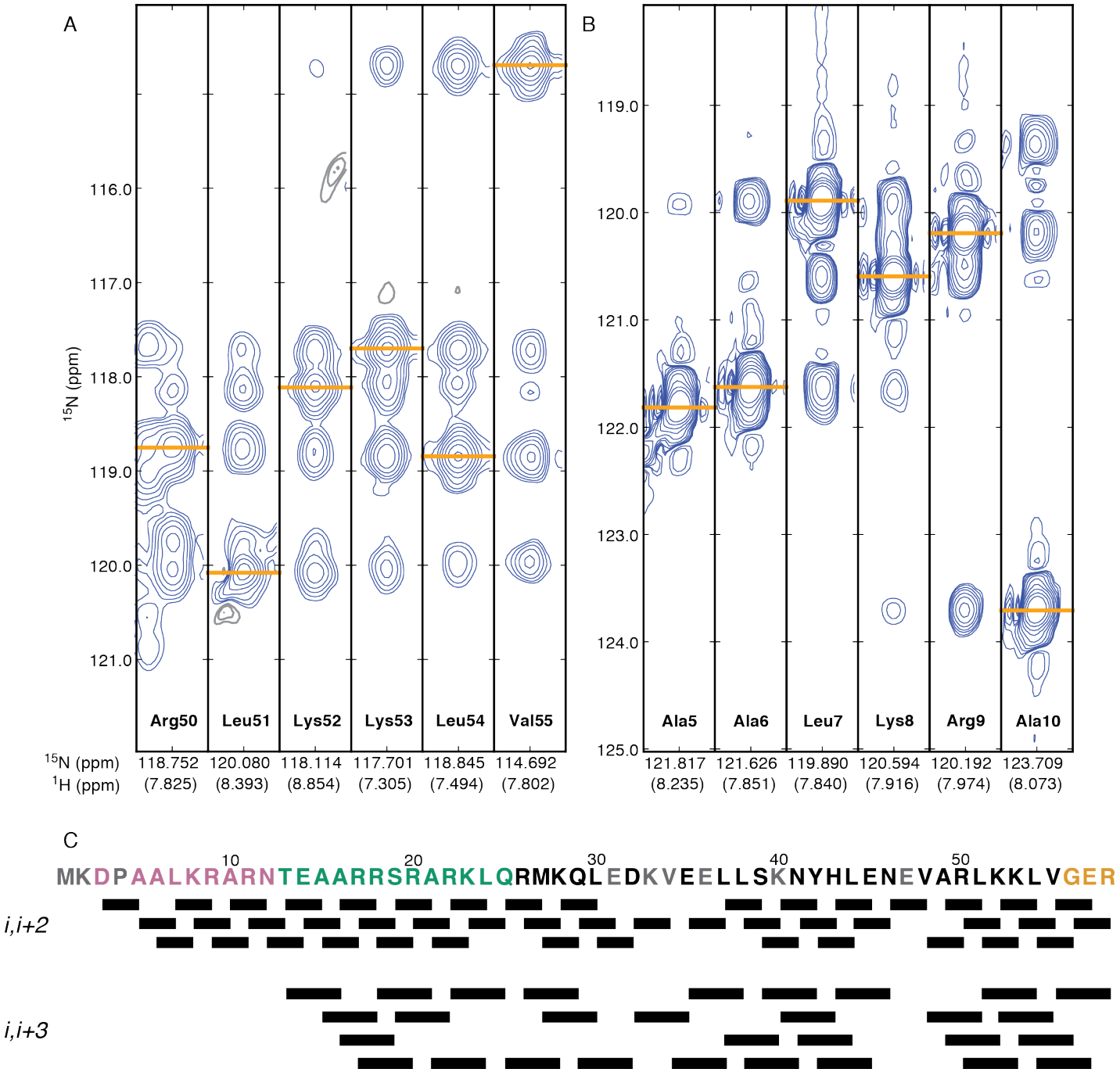

Figure S1. Representative strip plots of U-[^{15}N, ^{2}H] GCN4 (**A**) coiled-coil region and (**B**) basic region from an ^{1}H, ^{15}N, ^{15}N HSQC-NOESY-HSQC with 600 ms mixing time. NOE connectivities for i_{-3} to i_{+3} can be observed in panel A, while the connectivities in the disordered region (panel B) tends to only extend from i_{-2} to i_{+2}. Positive and negative contours are shown in blue and black, respectively. (**C**) All connectivities for i,i_{+2} and i,i_{+3} are shown. Residues are colored as described in the main text, except for those that were excluded from relaxation analysis and are shown in gray.

Figure S2

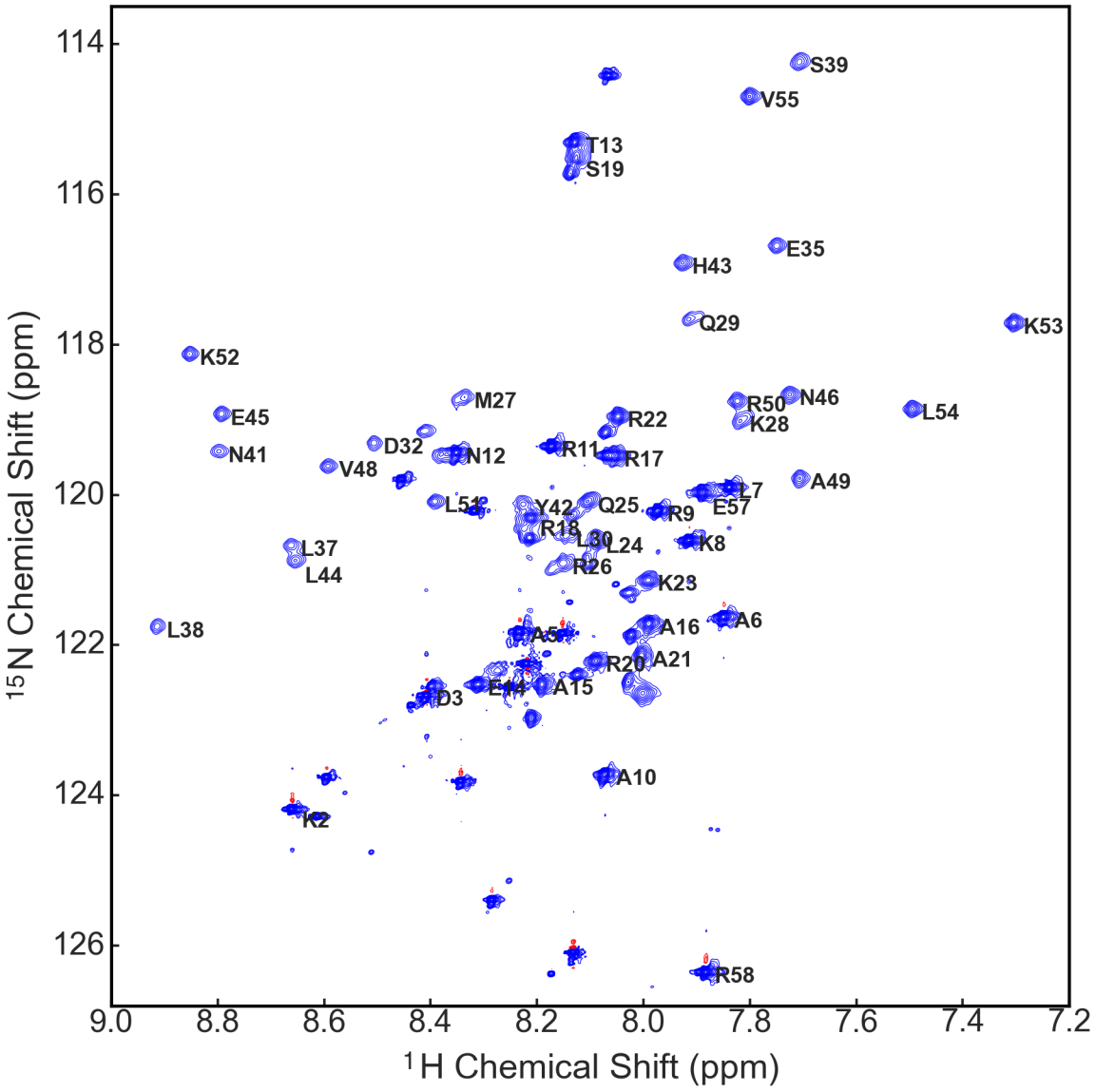

Figure S2. ^{1}H-^{15}N HSQC spectrum of U-[^{15}N, ^{2}H] GCN4. Unlabeled peaks correspond to small amounts of proteolysis during expression and purification in the basic region of GCN4.

Figure S3

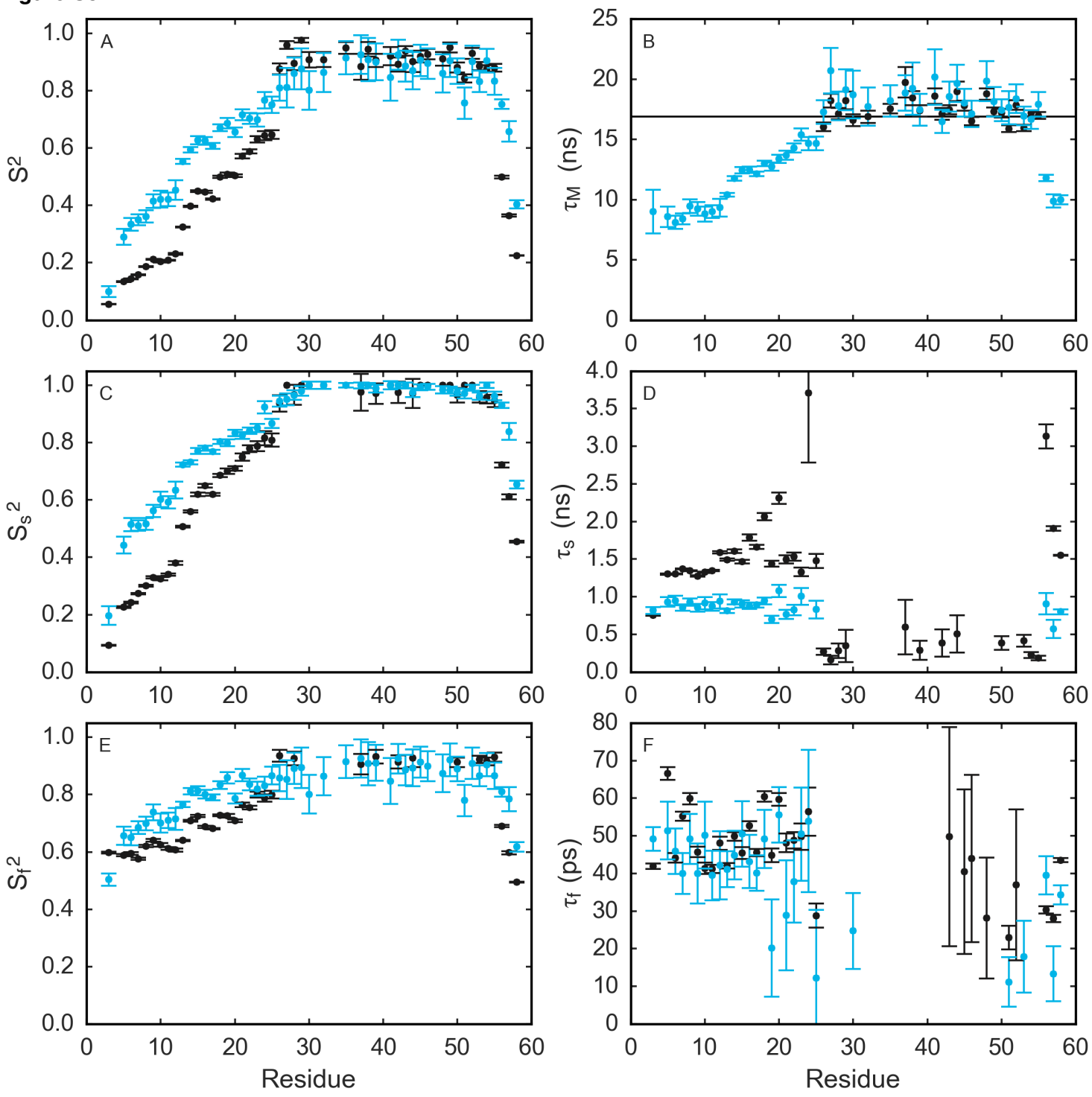

Figure S3. Comparison of Model-free parameters (**A**) S^2, (**B**) τ_M, (**C**) S_s^2, (**D**) τ_s, (**E**) S_f^2, and (**F**) τ_f determined from spectral density calculations (blue) and from analysis using the program relax with a fixed τ_M for disordered residues in the basic and C-terminal domains (black). The mean τ_M (16.9 ns) is indicated with a straight, black line.

Table S1. Time points used for measuring R_1 and R_2 relaxation rate constants of GCN4[1]

Experiment	B0 Field (T)	Time Points (s)
R_1	14.1	**0.02**, 0.06, **0.14**, 0.23, **0.34**, 0.47, 0.69, **0.98**, 1.50
	16.45	**0.02**, 0.14, **0.23**, 0.47, **0.98**, 1.50, 1.75
	18.8	**0.02**, 0.06, **0.08**, 0.14, **0.23**, 0.47, **0.98**, 1.50, 1.75
	21.1	**0.02**, 0.14, 0.23, **0.47**, **0.98**, 1.50
R_2	14.1	0.004, **0.008**, **0.024**, **0.064**, 0.096, **0.144**, 0.208
	16.45	0.004, **0.008**, 0.024, **0.064**, 0.096, **0.144**, 0.208
	18.8	0.004, **0.008**, **0.024**, **0.064**, 0.096, **0.144**, 0.208
	21.1	0.004, **0.008**, 0.024, **0.064**, 0.096, **0.144**, 0.208

[1]Time points that were collected in duplicate for error analysis are shown in bold.

Table S2. Amide chemical shifts for U-[^{15}N, ^{2}H] GCN4

Residue		^{1}H (ppm)	^{15}N (ppm)	Residue		^{1}H (ppm)	^{15}N (ppm)
1	M			**30**	L	8.14	120.5
2	K			**31**	E		
3	D	8.40	122.6	**32**	D	8.51	119.3
4	P			**33**	K		
5	A	8.23	121.8	**34**	V		
6	A	7.85	121.6	**35**	E	7.75	116.7
7	L	7.84	119.9	**36**	E		
8	K	7.92	120.6	**37**	L	8.66	120.7
9	R	7.97	120.2	**38**	L	8.91	121.7
10	A	8.07	123.7	**39**	S	7.71	114.2
11	R	8.17	119.3	**40**	K		
12	N	8.35	119.4	**41**	N	8.80	119.4
13	T	8.13	115.3	**42**	Y	8.22	120.1
14	E	8.31	122.5	**43**	H	7.93	116.9
15	A	8.19	122.5	**44**	L	8.65	120.9
16	A	7.99	121.7	**45**	E	8.79	118.9
17	R	8.06	119.5	**46**	N	7.72	118.7
18	R	8.21	120.3	**47**	E		
19	S	8.13	115.5	**48**	V	8.59	119.6
20	R	8.09	122.2	**49**	A	7.71	119.8
21	A	8.05	122.2	**50**	R	7.82	118.8
22	R	8.02	120.7	**51**	L	8.39	120.1
23	K	8.02	119.9	**52**	K	8.85	118.1
24	L	8.09	120.6	**53**	K	7.30	117.7
25	Q	8.10	120.1	**54**	L	7.49	118.9
26	R	8.15	120.9	**55**	V	7.80	114.7
27	M	8.33	118.7	**56**	G	7.79	108.5
28	K	7.82	119.0	**57**	E	7.89	120.0
29	Q	7.92	117.7	**58**	R	7.88	126.3

[1]Resonance assignments were determined from a ^{1}H, ^{15}N, ^{15}N HSQC-NOESY-HSQC with 600 ms mixing time.

Table S3. Relaxation parameters determined for GCN4 at 300 K[1]

Residue	14.1 T			16.45 T		
	R_1 (s^{-1})	R_2 (s^{-1})	NOE	R_1 (s^{-1})	R_2 (s^{-1})	NOE
3	1.11 ± 0.02	3.05 ± 0.38	-0.76 ± 0.01	1.07 ± 0.03	1.48 ± 0.11	-0.41 ± 0.01
5	1.38 ± 0.05	4.97 ± 0.84	-0.14 ± 0.01	1.35 ± 0.07	5.84 ± 0.31	0.06 ± 0.01
6	1.39 ± 0.04	5.80 ± 1.15	-0.01 ± 0.01	1.27 ± 0.07	6.02 ± 0.33	0.13 ± 0.01
7	1.37 ± 0.03	6.01 ± 0.97	-0.05 ± 0.01	1.32 ± 0.07	5.72 ± 0.29	0.10 ± 0.01
8	1.38 ± 0.03	6.09 ± 1.07	-0.03 ± 0.01	1.31 ± 0.07	8.34 ± 0.37	0.11 ± 0.01
9	1.39 ± 0.04	6.69 ± 1.23	0.02 ± 0.01	1.33 ± 0.09	7.58 ± 0.38	0.17 ± 0.01
10	1.39 ± 0.05	7.05 ± 1.56	0.06 ± 0.01	1.25 ± 0.10	7.50 ± 0.52	0.18 ± 0.01
11	1.36 ± 0.04	7.02 ± 1.30	0.06 ± 0.01	1.25 ± 0.08	7.54 ± 0.40	0.19 ± 0.01
12	1.36 ± 0.06	7.66 ± 2.04	0.14 ± 0.01	1.26 ± 0.11	7.75 ± 0.61	0.32 ± 0.01
13	1.27 ± 0.01	9.96 ± 0.29	0.18 ± 0.01	1.18 ± 0.03	10.26 ± 0.24	0.26 ± 0.01
14	1.28 ± 0.01	10.75 ± 0.33	0.26 ± 0.01	1.12 ± 0.04	12.00 ± 0.32	0.42 ± 0.01
15	1.20 ± 0.02	12.48 ± 0.54	0.27 ± 0.01	1.10 ± 0.05	12.39 ± 0.47	0.26 ± 0.01
16	1.17 ± 0.01	12.72 ± 0.55	0.27 ± 0.01	0.99 ± 0.04	14.19 ± 0.50	0.36 ± 0.01
17	1.18 ± 0.01	11.27 ± 0.33	0.27 ± 0.01	1.06 ± 0.02	12.20 ± 0.27	0.35 ± 0.01
18	1.18 ± 0.01	13.45 ± 0.53	0.34 ± 0.01	1.01 ± 0.03	14.61 ± 0.47	0.43 ± 0.01
19	1.14 ± 0.02	13.95 ± 0.87	0.28 ± 0.01	0.98 ± 0.06	14.68 ± 0.73	0.36 ± 0.02
20	1.10 ± 0.02	13.53 ± 0.67	0.35 ± 0.01	1.12 ± 0.05	12.94 ± 0.46	0.29 ± 0.01
21	1.09 ± 0.02	14.66 ± 1.09	0.34 ± 0.01	1.06 ± 0.08	15.45 ± 0.94	0.42 ± 0.02
22	1.04 ± 0.02	15.11 ± 1.08	0.35 ± 0.01	0.96 ± 0.06	16.94 ± 0.87	0.38 ± 0.02
23	1.01 ± 0.02	16.26 ± 1.27	0.36 ± 0.01	0.94 ± 0.07	19.13 ± 1.30	0.43 ± 0.02
24	1.01 ± 0.03	16.50 ± 1.96	0.52 ± 0.01	0.86 ± 0.09	18.84 ± 1.77	0.53 ± 0.03
25	1.01 ± 0.03	15.74 ± 1.85	0.49 ± 0.01	0.87 ± 0.09	17.97 ± 1.63	0.52 ± 0.03
26	0.82 ± 0.04	19.83 ± 2.78	0.58 ± 0.01	0.77 ± 0.09	22.63 ± 2.48	0.40 ± 0.03
27	0.71 ± 0.05	23.08 ± 4.40	0.68 ± 0.01	0.62 ± 0.09	28.91 ± 4.47	0.67 ± 0.03
28	0.77 ± 0.05	21.53 ± 3.67	0.69 ± 0.01	0.67 ± 0.07	24.54 ± 2.52	0.74 ± 0.03
29	0.75 ± 0.06	23.27 ± 5.89	0.72 ± 0.01	0.60 ± 0.12	27.36 ± 5.67	0.77 ± 0.04

30	0.75 ± 0.06	19.95 ± 3.30	0.80 ± 0.01	0.63 ± 0.07	23.50 ± 2.22	0.72 ± 0.02
32	0.76 ± 0.07	22.55 ± 3.82	0.78 ± 0.01	0.63 ± 0.07	25.54 ± 2.90	0.83 ± 0.02
35	0.75 ± 0.06	23.96 ± 3.43	0.78 ± 0.01	0.64 ± 0.05	26.17 ± 1.99	0.80 ± 0.02
37	0.69 ± 0.06	25.06 ± 4.19	0.74 ± 0.01	0.61 ± 0.06	29.23 ± 3.15	0.78 ± 0.02
38	0.73 ± 0.07	24.45 ± 4.07	0.86 ± 0.01	0.64 ± 0.06	26.73 ± 2.61	0.75 ± 0.02
39	0.77 ± 0.06	22.04 ± 3.40	0.71 ± 0.01	0.69 ± 0.06	24.83 ± 2.30	0.71 ± 0.02
41	0.69 ± 0.07	27.21 ± 5.27	0.80 ± 0.01	0.58 ± 0.07	27.47 ± 3.12	0.85 ± 0.03
42	0.78 ± 0.05	20.88 ± 2.58	0.73 ± 0.01	0.72 ± 0.06	22.46 ± 1.72	0.75 ± 0.02
43	0.75 ± 0.05	23.21 ± 2.98	0.77 ± 0.01	0.66 ± 0.05	25.80 ± 1.79	0.74 ± 0.02
44	0.70 ± 0.06	24.40 ± 3.37	0.72 ± 0.01	0.61 ± 0.05	28.37 ± 2.67	0.77 ± 0.02
45	0.73 ± 0.05	25.51 ± 3.26	0.72 ± 0.01	0.68 ± 0.05	26.32 ± 1.90	0.77 ± 0.02
46	0.78 ± 0.06	22.15 ± 2.76	0.75 ± 0.01	0.71 ± 0.05	24.22 ± 1.69	0.75 ± 0.02
48	0.68 ± 0.06	23.91 ± 3.37	0.76 ± 0.01	0.60 ± 0.05	26.94 ± 2.38	0.71 ± 0.02
49	0.77 ± 0.06	23.39 ± 2.95	0.75 ± 0.01	0.69 ± 0.05	25.44 ± 1.96	0.73 ± 0.02
50	0.76 ± 0.05	22.68 ± 2.33	0.69 ± 0.01	0.66 ± 0.04	24.53 ± 1.52	0.74 ± 0.01
51	0.74 ± 0.06	21.50 ± 2.04	0.74 ± 0.01	0.59 ± 0.05	22.85 ± 1.55	0.76 ± 0.02
52	0.75 ± 0.06	23.70 ± 2.73	0.74 ± 0.01	0.62 ± 0.05	25.92 ± 1.71	0.78 ± 0.01
53	0.82 ± 0.04	20.12 ± 1.67	0.68 ± 0.01	0.69 ± 0.03	22.32 ± 0.97	0.70 ± 0.01
54	0.73 ± 0.04	22.90 ± 2.12	0.65 ± 0.01	0.76 ± 0.04	24.13 ± 1.36	0.65 ± 0.01
55	0.74 ± 0.05	21.63 ± 2.08	0.63 ± 0.01	0.68 ± 0.04	22.34 ± 1.23	0.61 ± 0.01
56	1.04 ± 0.02	13.71 ± 0.52	0.54 ± 0.01	1.03 ± 0.02	14.69 ± 0.29	0.56 ± 0.01
57	1.13 ± 0.07	10.12 ± 2.17	0.36 ± 0.01	1.10 ± 0.05	11.33 ± 0.44	0.42 ± 0.01
58	1.10 ± 0.03	6.74 ± 0.53	-0.01 ± 0.01	0.99 ± 0.02	6.31 ± 0.10	0.08 ± 0.01

[1] R_1 and R_2 spin relaxation rates at 16.45 T are adjusted for temperature as noted in the text.

Table S3 (continued)

Residue	18.8 T			21.1 T		
	R_1 (s^{-1})	R_2 (s^{-1})	NOE	R_1 (s^{-1})	R_2 (s^{-1})	NOE
3	1.09 ± 0.07	3.59 ± 0.04	-0.18 ± 0.01	1.18 ± 0.01	2.16 ± 0.07	-0.02 ± 0.01
5	1.24 ± 0.14	6.91 ± 0.11	0.14 ± 0.01	1.34 ± 0.01	5.92 ± 0.04	0.29 ± 0.01
6	1.25 ± 0.16	6.20 ± 0.13	0.27 ± 0.01	1.28 ± 0.02	6.33 ± 0.05	0.33 ± 0.01
7	1.26 ± 0.13	7.42 ± 0.12	0.20 ± 0.01	1.25 ± 0.01	6.70 ± 0.04	0.34 ± 0.01
8	1.27 ± 0.15	7.40 ± 0.13	0.22 ± 0.01	1.29 ± 0.01	7.71 ± 0.05	0.35 ± 0.01
9	1.22 ± 0.17	8.12 ± 0.16	0.29 ± 0.01	1.24 ± 0.02	8.41 ± 0.06	0.39 ± 0.01
10	1.26 ± 0.22	8.46 ± 0.22	0.32 ± 0.01	1.22 ± 0.02	8.09 ± 0.08	0.35 ± 0.01
11	1.24 ± 0.18	8.28 ± 0.15	0.31 ± 0.01	1.19 ± 0.01	8.22 ± 0.06	0.39 ± 0.01
12	1.13 ± 0.22	8.97 ± 0.23	0.32 ± 0.01	1.18 ± 0.02	9.04 ± 0.09	0.42 ± 0.01
13	1.10 ± 0.04	11.00 ± 0.08	0.35 ± 0.01	1.02 ± 0.01	11.71 ± 0.06	0.42 ± 0.02
14	1.04 ± 0.05	13.18 ± 0.13	0.40 ± 0.01	1.07 ± 0.01	14.13 ± 0.09	0.48 ± 0.02
15	1.00 ± 0.07	14.92 ± 0.20	0.41 ± 0.01	0.98 ± 0.01	15.47 ± 0.13	0.47 ± 0.02
16	0.98 ± 0.06	14.61 ± 0.22	0.36 ± 0.01	0.94 ± 0.01	15.41 ± 0.13	0.47 ± 0.02
17	1.07 ± 0.04	13.89 ± 0.14	0.38 ± 0.01	0.95 ± 0.01	14.73 ± 0.09	0.49 ± 0.01
18	0.91 ± 0.05	16.16 ± 0.20	0.39 ± 0.01	0.94 ± 0.01	17.23 ± 0.14	0.50 ± 0.02
19	0.99 ± 0.07	16.54 ± 0.33	0.39 ± 0.01	0.85 ± 0.01	17.03 ± 0.21	0.56 ± 0.03
20	0.96 ± 0.05	16.57 ± 0.26	0.37 ± 0.01	0.89 ± 0.01	17.39 ± 0.18	0.49 ± 0.02
21	0.89 ± 0.09	18.14 ± 0.44	0.43 ± 0.01	0.82 ± 0.01	19.13 ± 0.29	0.57 ± 0.03
22	0.81 ± 0.07	18.94 ± 0.39	0.41 ± 0.01	0.79 ± 0.01	19.39 ± 0.25	0.52 ± 0.03
23	0.83 ± 0.09	19.29 ± 0.55	0.44 ± 0.01	0.80 ± 0.01	20.93 ± 0.40	0.48 ± 0.03
24	0.84 ± 0.16	20.88 ± 0.81	0.49 ± 0.01	0.74 ± 0.02	21.54 ± 0.55	0.55 ± 0.05
25	0.80 ± 0.12	20.06 ± 0.79	0.57 ± 0.01	0.74 ± 0.02	21.32 ± 0.59	0.69 ± 0.05
26	0.68 ± 0.12	27.08 ± 1.53	0.60 ± 0.01	0.56 ± 0.02	26.10 ± 1.01	0.68 ± 0.06
27	0.62 ± 0.14	29.90 ± 2.37	0.67 ± 0.01	0.51 ± 0.03	31.83 ± 2.04	0.77 ± 0.06
28	0.62 ± 0.08	27.40 ± 1.94	0.70 ± 0.01	0.49 ± 0.02	29.19 ± 1.43	0.80 ± 0.04

Residue	18.8 T			21.1 T		
	R_1 (s^{-1})	R_2 (s^{-1})	NOE	R_1 (s^{-1})	R_2 (s^{-1})	NOE
29	0.57 ± 0.14	29.82 ± 2.92	0.76 ± 0.01	0.49 ± 0.03	31.86 ± 2.30	0.72 ± 0.06
30	0.59 ± 0.09	28.01 ± 2.33	0.80 ± 0.01	0.52 ± 0.03	28.66 ± 1.64	0.71 ± 0.04
32	0.59 ± 0.08	27.60 ± 2.09	0.78 ± 0.01	0.49 ± 0.03	28.80 ± 1.47	0.78 ± 0.03
35	0.61 ± 0.05	30.14 ± 1.68	0.84 ± 0.01	0.48 ± 0.02	31.46 ± 1.33	0.67 ± 0.03
37	0.54 ± 0.07	32.60 ± 2.59	0.80 ± 0.01	0.41 ± 0.03	32.06 ± 1.80	0.74 ± 0.03
38	0.54 ± 0.08	31.31 ± 2.55	0.66 ± 0.02	0.47 ± 0.03	33.63 ± 1.89	0.84 ± 0.04
39	0.58 ± 0.06	27.78 ± 1.66	0.73 ± 0.01	0.48 ± 0.02	30.13 ± 1.39	0.73 ± 0.03
41	0.56 ± 0.10	32.03 ± 3.14	0.74 ± 0.02	0.46 ± 0.03	31.65 ± 1.99	0.81 ± 0.05
42	0.64 ± 0.07	27.32 ± 1.56	0.76 ± 0.01	0.46 ± 0.02	29.93 ± 1.30	0.81 ± 0.03
43	0.62 ± 0.05	27.94 ± 1.50	0.72 ± 0.01	0.50 ± 0.02	32.34 ± 1.26	0.76 ± 0.03
44	0.55 ± 0.07	31.77 ± 2.56	0.76 ± 0.01	0.46 ± 0.03	31.86 ± 1.56	0.78 ± 0.03
45	0.57 ± 0.06	29.53 ± 1.93	0.70 ± 0.01	0.46 ± 0.02	30.57 ± 1.34	0.76 ± 0.03
46	0.62 ± 0.05	26.86 ± 1.38	0.72 ± 0.01	0.51 ± 0.02	29.44 ± 1.07	0.79 ± 0.03
48	0.53 ± 0.06	29.54 ± 2.06	0.74 ± 0.01	0.44 ± 0.02	33.06 ± 1.51	0.79 ± 0.03
49	0.58 ± 0.05	30.17 ± 1.56	0.73 ± 0.01	0.50 ± 0.02	30.91 ± 1.27	0.79 ± 0.02
50	0.59 ± 0.04	26.73 ± 1.20	0.72 ± 0.01	0.48 ± 0.01	28.73 ± 0.89	0.75 ± 0.02
51	0.58 ± 0.05	23.31 ± 0.76	0.68 ± 0.01	0.50 ± 0.02	25.49 ± 0.58	0.80 ± 0.03
52	0.61 ± 0.06	28.16 ± 1.71	0.75 ± 0.01	0.47 ± 0.02	32.43 ± 1.33	0.77 ± 0.02
53	0.61 ± 0.03	24.76 ± 0.77	0.72 ± 0.01	0.55 ± 0.01	27.28 ± 0.67	0.72 ± 0.02
54	0.59 ± 0.04	27.07 ± 0.92	0.66 ± 0.01	0.47 ± 0.01	28.20 ± 0.82	0.65 ± 0.02
55	0.59 ± 0.04	26.59 ± 1.07	0.61 ± 0.01	0.50 ± 0.02	29.02 ± 0.84	0.69 ± 0.02
56	0.90 ± 0.02	16.14 ± 0.26	0.55 ± 0.01	0.74 ± 0.01	17.18 ± 0.18	0.59 ± 0.01
57	0.94 ± 0.07	12.25 ± 0.36	0.44 ± 0.01	0.83 ± 0.02	12.85 ± 0.14	0.53 ± 0.01
58	0.96 ± 0.03	9.37 ± 0.11	0.14 ± 0.01	0.93 ± 0.01	8.46 ± 0.03	0.26 ± 0.01

Table S4. Model-free parameters for GCN4 determined using the program *relax*[1]

Residue	Model	χ^2	τ_M (ns)	S^2	τ_f (ps)	S_f^2	τ_s (ns)	S_s^2 (S^2/S_f^2)
3	6	588.33		0.06 ± 0.01	41.93 ± 0.70	0.60 ± 0.01	0.75 ± 0.01	0.09 ± 0.01
5	6	268.30		0.13 ± 0.01	66.59 ± 1.71	0.59 ± 0.01	1.30 ± 0.01	0.23 ± 0.01
6	6	30.69		0.14 ± 0.01	44.14 ± 1.24	0.60 ± 0.01	1.30 ± 0.01	0.24 ± 0.01
7	6	171.52		0.16 ± 0.01	55.22 ± 1.24	0.58 ± 0.01	1.37 ± 0.01	0.27 ± 0.01
8	6	54.33		0.19 ± 0.01	59.86 ± 1.54	0.62 ± 0.01	1.35 ± 0.01	0.30 ± 0.01
9	6	30.64		0.21 ± 0.01	45.71 ± 1.40	0.64 ± 0.01	1.28 ± 0.01	0.33 ± 0.01
10	6	50.12		0.20 ± 0.01	41.34 ± 1.48	0.62 ± 0.01	1.33 ± 0.01	0.33 ± 0.01
11	6	35.97		0.21 ± 0.01	41.21 ± 1.10	0.61 ± 0.01	1.35 ± 0.01	0.34 ± 0.01
12	6	122.29		0.23 ± 0.01	48.03 ± 1.75	0.61 ± 0.01	1.59 ± 0.01	0.38 ± 0.01
13	6	189.80		0.32 ± 0.01	41.98 ± 0.73	0.64 ± 0.01	1.49 ± 0.01	0.51 ± 0.01
14	6	74.95		0.40 ± 0.01	49.84 ± 1.16	0.71 ± 0.01	1.60 ± 0.02	0.56 ± 0.01
15	6	68.07		0.45 ± 0.01	45.37 ± 1.56	0.72 ± 0.01	1.47 ± 0.03	0.62 ± 0.01
16	6	55.95		0.45 ± 0.01	52.62 ± 1.25	0.69 ± 0.01	1.79 ± 0.04	0.65 ± 0.01
17	6	69.38		0.42 ± 0.01	45.51 ± 0.95	0.68 ± 0.01	1.66 ± 0.03	0.62 ± 0.01
18	6	59.28		0.50 ± 0.01	60.45 ± 1.43	0.73 ± 0.01	2.06 ± 0.05	0.69 ± 0.01
19	6	59.24		0.51 ± 0.01	44.81 ± 1.84	0.73 ± 0.01	1.44 ± 0.04	0.70 ± 0.01
20	6	76.92		0.50 ± 0.01	59.67 ± 1.65	0.71 ± 0.01	2.31 ± 0.07	0.71 ± 0.01
21	6	30.72		0.57 ± 0.01	48.09 ± 2.48	0.76 ± 0.01	1.50 ± 0.05	0.75 ± 0.01
22	6	26.61		0.59 ± 0.01	48.77 ± 2.17	0.76 ± 0.01	1.53 ± 0.06	0.78 ± 0.01
23	6	3.34		0.63 ± 0.01	49.78 ± 3.48	0.80 ± 0.01	1.33 ± 0.06	0.79 ± 0.02
24	6	6.39		0.64 ± 0.02	56.41 ± 6.37	0.79 ± 0.01	3.71 ± 0.93	0.82 ± 0.02
25	6	6.77		0.65 ± 0.01	28.78 ± 3.17	0.80 ± 0.01	1.48 ± 0.09	0.81 ± 0.02
26	5	60.71	16.04 ± 0.36	0.88 ± 0.02		0.94 ± 0.02	0.27 ± 0.04	0.94 ± 0.03
27	2	9.87	18.21 ± 0.56	0.96 ± 0.01			0.16 ± 0.06	
28	5	15.94	17.13 ± 0.47	0.90 ± 0.02		0.93 ± 0.02	0.28 ± 0.10	0.97 ± 0.03
29	2	4.43	18.22 ± 0.74	0.98 ± 0.01			0.35 ± 0.21	
30	2	66.30	16.59 ± 0.49	0.91 ± 0.03	22.51 ± 28.86			

Residue	Model	χ^2	τ_M (ns)	S^2	τ_f (ps)	S_f^2	τ_s (ns)	S_s^2 (S^2/S_f^2)
32	2	3.05	16.89 ± 0.50	0.91 ± 0.03	19.37 ± 27.00			
35	2	48.38	17.55 ± 0.39	0.95 ± 0.02	28.02 ± 45.44			
37	5	9.60	19.74 ± 1.26	0.88 ± 0.05		0.91 ± 0.04	0.59 ± 0.36	0.98 ± 0.06
38	2	102.63	18.43 ± 0.58	0.94 ± 0.03	30.83 ± 83.09			
39	5	1.34	17.37 ± 0.48	0.91 ± 0.02		0.93 ± 0.02	0.29 ± 0.13	0.97 ± 0.04
41	2	11.34	18.60 ± 0.65	0.92 ± 0.03	21.42 ± 57.64			
42	5	9.45	17.12 ± 0.49	0.89 ± 0.03		0.91 ± 0.02	0.39 ± 0.18	0.98 ± 0.04
43	2	15.37	17.47 ± 0.39	0.94 ± 0.02	49.78 ± 29.10			
44	5	3.10	18.98 ± 0.81	0.90 ± 0.04		0.93 ± 0.03	0.50 ± 0.25	0.97 ± 0.05
45	2	23.27	17.82 ± 0.42	0.92 ± 0.02	40.50 ± 21.86			
46	2	11.43	16.52 ± 0.33	0.93 ± 0.02	43.96 ± 22.27			
48	2	7.37	18.78 ± 0.47	0.91 ± 0.02	28.12 ± 16.06			
49	2	15.65	17.30 ± 0.36	0.95 ± 0.02	58.11 ± 43.61			
50	5	5.26	17.18 ± 0.35	0.88 ± 0.02		0.91 ± 0.02	0.38 ± 0.09	0.97 ± 0.03
51	2	23.44	15.88 ± 0.28	0.84 ± 0.01	22.90 ± 3.15			
52	2	8.56	17.85 ± 0.40	0.93 ± 0.02	36.95 ± 20.08			
53	5	8.18	15.95 ± 0.26	0.89 ± 0.01		0.92 ± 0.01	0.41 ± 0.08	0.96 ± 0.02
54	5	26.87	17.19 ± 0.26	0.88 ± 0.01		0.92 ± 0.01	0.23 ± 0.04	0.96 ± 0.02
55	5	15.15	16.99 ± 0.29	0.88 ± 0.01		0.93 ± 0.02	0.18 ± 0.03	0.95 ± 0.02
56	6	55.91		0.50 ± 0.01	30.34 ± 0.99	0.69 ± 0.01	3.13 ± 0.16	0.72 ± 0.01
57	6	102.05		0.36 ± 0.01	28.05 ± 0.99	0.60 ± 0.01	1.91 ± 0.03	0.61 ± 0.01
58	6	598.91		0.22 ± 0.01	43.53 ± 0.54	0.49 ± 0.01	1.55 ± 0.01	0.45 ± 0.01

[1]Relaxation data were analyzed with a fixed τ_M for the basic and disordered C-terminal regions. Input data were from R_1, R_2, and $\{^1H\}$-^{15}N heteronuclear NOE rate constants determined at 14.1, 16.45, 18.8, and 21.1 T.